Received: 19 May 2023 | Revised: 23 September 2023 | Accepted: 28 October 2023

IET Generation, Transmission & Distribution

DOI: 10.1049/gtd2.13058

The Institution of Engineering and Technology WILEY

ORIGINAL RESEARCH

Fueling the seaport of the future: Investments in low-carbon energy technologies for operational resilience in seaport multi-energy systems

Chengzhi Xie[1] | **Payman Dehghanian**[1] | **Abouzar Estebsari**[2]

[1]Department of Electrical and Computer Engineering, George Washington University, Washington, District of Columbia, USA

[2]School of the Built Environment and Architecture, London South Bank University, London, UK

Correspondence
Payman Dehghanian, Department of Electrical and Computer Engineering, George Washington University, Washington, D.C. 20052, USA.
Email: payman@gwu.edu

Funding information
National Science Foundation, Grant/Award Number: ECCS-2114100

Abstract

The ability to withstand and recover from disruptions is essential for seaport energy systems, and in light of the growing push for decarbonization, incorporating clean energy sources has become increasingly imperative to ensure resilience. This paper proposes a resilience enhancement planning strategy for a seaport multi-energy system that integrates various energy modalities and sources, including heating, cooling, hydrogen, solar, and wind power. The planning strategy aims to ensure the reliable operation of the system during contingency events, such as power outages, equipment failures, or extreme weather incidents. The proposed optimization model is designed as a mixed-integer nonlinear programming formulation, in which McCormick inequalities and other linearization techniques are utilized to tackle the model nonlinearities. The model allocates fuel cell electric trucks (FCETs), renewable energy sources, hydrogen refueling stations, and remote control switches such that the system resilience is enhanced while incorporating natural-gas-powered combined cooling, heating, and power system to minimize the operation and unserved demand costs. The model considers various factors such as the availability of renewable energy sources, the demand for heating, cooling, electricity, and hydrogen, the operation of remote control switches to help system reconfiguration, the travel behaviour of FCETs, and the power output of FCETs via vehicle-to-grid interface. The numerical results demonstrate that the proposed strategy can significantly improve the resilience of the seaport multi-energy system and reduce the risk of service disruptions during contingency scenarios.

1 | INTRODUCTION

1.1 | Motivation and rationale

Seaports are known to be energy-intensive, due to the presence of various heavy machinery and equipment used for loading and unloading cargo. The demand for electricity in seaports is further increased by the need for lighting, refrigeration, and other climate control systems [1]. Aside from power demand, seaports are also attributed to high demands for cooling and heating energy, making it challenging to ensure a stable energy supply [2–4]. Despite the critical role that seaports play in our economy, they continuously face a multitude of risks, including natural disasters such as hurricanes, floods, typhoons, earthquakes, and fires, as well as operational failures, which, if realized, can disrupt their functions and cause significant socio-economic consequences. Therefore, more efficient and sustainable power, cooling, and heating solutions that can reduce the seaport's reliance on traditional energy sources and improve its energy resilience are urgently needed.

Seaport multi-energy systems are inherently more complex than a conventional power distribution system, involving the integration of multiple forms of energy—electricity, gas, water, and sometimes even heat—alongside various other logistical and operational components. These systems not only have to ensure energy resilience but also need to account for the

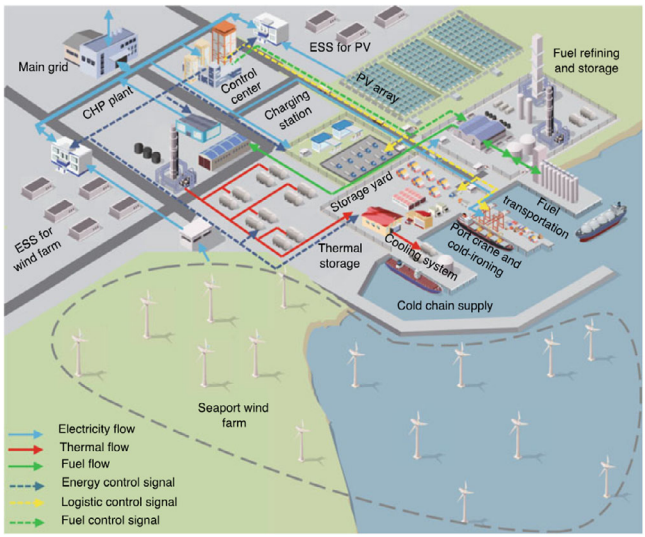

FIGURE 1 A typical topology of future seaport microgrid [3].

interdependencies between different energy vectors and other seaport operations. Additionally, the governance and decision-making processes can be more complicated due to the involvement of multi-stakeholders, including private seaport owners who have the autonomy to make technology choices [5]. As can be seen in Figure 1, the seaport system is geographically more limited than a conventional power distribution system but features higher density, caters to specialized operations, and is subject to unique risks such as hurricanes and sabotage. Therefore, resilience in seaport multi-energy systems requires a more holistic, multi-disciplinary approach that considers both technical and organizational complexities. Enhancing seaport operational resilience through multi-energy systems ensures reliable operation during contingency scenarios. Multi-energy systems integrate various energy sources, including heating, cooling, hydrogen, natural gas, solar, and wind power, providing a more flexible and reliable supply of energy to seaport systems [6–8]. The combined cooling, heating, and power (CCHP) system, powered by natural gas, is a highly efficient and low-carbon emission stationary distributed energy resource (DER) [9, 10]. In addition to supplying electrical energy to the system, it also has the capability to provide heating and cooling energy. This makes it a versatile and valuable asset for enhancing the reliability and resilience of the seaport energy system [11]. By providing multiple forms of energy, the CCHP system can mitigate the impacts of potential disruptions in the system driven by random contingencies or natural disasters. Furthermore, the high efficiency of the CCHP system highlights that it can operate more reliably and cost-effectively than conventional power plants, further reducing the risk of power outages and energy shortages [12]. With intensified electrification in the transportation sector, new opportunities are provided for incorporating clean energy vehicles into the seaport transportation systems to reduce carbon emissions and promote sustainable practices in the shipping industry [13]. Electric vehicles and fuel cell (FC) vehicles are two viable options for seaport transportation. Electric vehicles are cost-effective and low-emission technologies, while FC vehicles emit zero harmful emissions and have longer ranges [14]. Note that FCETs fueled by hydrogen have advantages over battery-based clean-energy buses, such as longer ranges, shorter refueling periods, and faster discharging rates [15].

Hydrogen-based microgrids can integrate renewable-driven hydrogen production, FC stacks, and HRSs, serving as the interface that couples the transportation and modern energy network [16]. Hydrogen-based microgrids can aid utility planners in reducing carbon emissions and supporting local hydrogen vehicle owners [17]. Following a contingency event, FCETs can also serve as a reliable backup power supply for the electric system through V2G interfaces and increase the self-sustaining ability of each microgrid affected by the disaster [18]. The two-way flow of electricity can enhance the stability and resilience of the power grid. In addition to V2G facilities, installing RESs into the seaport system (e.g. wind turbine and photovoltaic array) can also enhance seaport operation performance [19]. These sources emit zero greenhouse gas emissions, are sustainable, and are widely available, making them ideal for powering hydrogen refueling stations in seaports [20]. By optimally allocating HRSs and RESs, FCETs in seaport systems are capable of picking up unserved loads via scheduled routing between V2G interfaces, further enhancing system resilience.

Beyond multi-energy systems in seaports and renewable-integrated hydrogen-based microgrids, investments in the installation of remote control switches (RCSs) across the network or upgrading manual switches to RCSs significantly contribute to service restoration efficiency and the resilience of the seaport PDN [21]. Hassanzadeh et al. [22] suggest that using RCSs can better prepare the PDN for possible fault scenarios caused by severe weather events. Additionally, [23] shows that using RCSs can reduce the interruption duration of the electric energy for customers through joint network reconfiguration and utilization of distributed generations and mobile emergency generators before and after natural calamities.

This paper's approach to improving the resilience of seaport energy systems is through joint planning and integration of multi-energy systems, FCETs, and RCSs. Each of these technologies, such as CCHP, HRSs, RESs, FCETs, and RCSs, contributes to the assurance of a reliable and flexible energy supply to the seaport PDN and supported consumers. This paper examines the effectiveness of this integration into the seaport system and verifies how emerging energy technologies can be optimally deployed to enhance the resilience of the system in the face of equipment failures and power outages, natural disasters, and other unforeseen disruptions.

1.2 | Literature review

In recent years, researchers have been exploring the electrification of seaport systems aiming to curtail carbon emissions, and the integration of multiple energy sources to optimize energy utilization [2, 4]. The traditional port systems operate with the segregation of energy sources for power, heating, and cooling, which are typically managed independently and operate

in separate networks, such as power, hydrogen, and gas systems. In [24], an innovative distributed algorithm is introduced to address the computational complexity associated with the simultaneous resolution of day-ahead operational planning and real-time decision-making for multi-energy system energy management. A dynamic optimal energy flow model is proposed in [6] to enhance the heat and electricity-integrated energy system with the participation of distributed RESs. According to Song et al. [25], a novel approach to enhance energy efficiency in seaports is to optimize and control various loads through innovative port system designs. Research has also been conducted on integrated power-gas systems (IPGSs). In [26], a security-constrained bilevel economic dispatch model is proposed to minimize the total production cost in an IPGS. To manage the operation of an IPGS, Khani et al. [27] developed an optimal day-ahead scheduling model. In [28], a robust scheduling model that accounts for the uncertainty of wind power is presented for an IPGS. Expanding the previous research, Wang et al. [8] proposes a novel energy supply structure for an integrated port energy system that incorporates multi-energy coupling associated with hydrogen.

To enhance the power distribution network (PDN) resilience, previous research has studied the critical role that DERs play in boosting the service restoration capacity and rapidity when facing disasters. A mathematical optimization approach is presented in [29] to restore critical loads in distribution systems utilizing DERs during disasters, while considering the capacity and availability of DERs, topology of the distribution system, and priority and location of critical loads. Ranjbar et al. [30] proposed a planning model for transmission systems and DERs that prioritizes resiliency under normal and emergency conditions, using Benders decomposition and pre-determined damage scenarios with improved computational performance. Zhang et al. [31] proposed a multi-objective optimization model for the optimal allocation of DERs to enhance the resilience of power systems during extreme events, considering capacity accessibility, prioritization of non-black start generating units, and economic cost and resilience trade-off. Strategic switch placement for achieving PDN reconfiguration and isolating the faults to reduce service interruption costs is also thoroughly researched in the literature. Arjomandi-Nezhad et al. [32] proposed a PDN recovery strategy through joint decisions on optimal switch placement and repair sequence plans on faulted elements. In [33], a methodology is introduced that utilizes smart control switches in coordination with energy storage systems to achieve faster fault isolation and service restoration. Izadi et al. [34] proposed a conditional value-at-risk constrained switch placement model for PDN resilience enhancement. More recently, mobile power sources (MPSs), i.e. mobile energy storage systems, FCETs, and truck-mounted mobile emergency generators, have been studied for enhancing PDN resilience during extremes. Amongst, [35] discussed the strategic use of MPSs and introduced optimization models for coordinated operation of MPSs with repair crews to improve power system resilience and restoration rapidity during extreme events, while authors in [36] further considered decision-dependent uncertainty in the availability of MPSs due to travel and waiting times. Li et al. [37] propose a two-stage optimization method for enhancing the PDN resilience against extreme weather events by pre-positioning emergency stations and co-dispatching mobile energy storage systems and repair crews on a transportation network. A two-stage robust optimization formulation with integer corrective decisions is presented to support the sustainability- and resilience-oriented planning of microgrid-aided bus centers [38]. A new rolling-horizon operation model for a fleet of truck-mounted mobile batteries is proposed in [39], which could switch between normal and emergency operating states by integrating a new schedule memory concept into the upcoming horizons, ensuring maximum resiliency at minimum cost.

1.3 | Contribution and paper structure

Beyond the state-of-the-art literature, this paper aims to provide a planning framework that decides on the effective integration of zero-carbon emission FCETs into the seaport energy systems as backup power sources for enhanced reliability and resilience. FCETs can be fueled by the HRS using different types of hydrogen generation practices such as on-site electrolyzers or industry-produced purified hydrogen. The HRS in this study includes renewable energy sources, on-site electrolyzers, on-site gas compressors, hydrogen storage tanks, hydrogen fuel dispensers, and on-site FCs. The initial investment cost of HRSs, RCSs, and FCETs can be offset by selling hydrogen generated by renewable energy to the local market. Meanwhile, the CCHP system provides cooling to the seaport cold-chain supply system and transfers heat to the workplaces. Under the occurrence of catastrophe events, the seaport PDN can rely on stationary DERs, such as the CCHP and HRSs, as well as the MPSs in the form of FCETs that can provide power to the grid through V2G interfaces. By coordinating the HRSs planning, FCETs scheduling, and the RCSs operation, the resilience of the seaport PDN can be significantly enhanced. We propose a scenario-based optimization model that effectively captures the prevailing uncertainties in the system and energy resources. In the planning stage, the model decides on the deployment of HRSs among predefined candidate nodes, the number of RESs to be located in each HRS facility, the number of FCETs to be purchased and utilized, and the number of RCSs to be installed at upstream or downstream branches. The objective of the proposed model is to minimize the capital investment cost on HRS/RES/RCS/FCET, the annualized maintenance and operation costs of the invested facilities, and the unserved energy demand costs under different contingency scenarios. Numerical results on the IEEE 33-Bus test system demonstrate the efficacy of the proposed model. The related literature is compared with the proposed model in Table 1.

The main contributions of this paper are listed as follows:

- This study proposes a planning framework for low-carbon integrated seaport multi-energy systems that mainly relies on renewable energy sources, such as hydrogen, natural gas, solar, and wind, to achieve decarbonization goals and

TABLE 1 Comparison of existing literature and the proposed model.

	Problem discription			Energy type/technology						Energy Storage		Reliability			
Ref.	System operation	System expansion planning	Uncertainty	Solar	Wind	Hydrogen	Natural gas	Heating	Cooling	Heating	Hydrogen	Fuel cell	Distributed energy resource	Remote control switch	Mobile power source
[6]	✓	×	×	✓	✓	×	✓	✓	×	✓	×	×	×	×	×
[25]	✓	✓	✓	×	✓	×	✓	✓	✓	×	×	×	×	×	×
[26]	✓	×	×	×	✓	×	✓	×	×	×	×	×	×	×	×
[27]	✓	×	✓	✓	✓	×	✓	×	×	×	×	×	×	×	×
[28]	✓	×	✓	×	✓	×	✓	×	×	×	×	×	×	×	×
[8]	✓	×	×	×	✓	✓	✓	✓	×	✓	✓	✓	×	×	×
[29]	✓	×	✓	×	×	×	×	×	×	×	×	×	✓	✓	×
[30]	✓	✓	✓	×	✓	×	×	×	×	×	×	×	✓	×	×
[31]	✓	✓	✓	✓	×	×	×	×	×	×	×	×	✓	×	×
[32]	✓	✓	×	×	×	×	×	×	×	×	×	×	✓	✓	×
[33]	✓	✓	✓	×	×	×	×	×	×	×	×	×	✓	✓	×
[34]	✓	✓	✓	×	×	×	×	×	×	×	×	×	×	✓	×
[35, 37]	✓	×	✓	×	×	×	×	×	×	×	×	×	×	×	✓
[38]	✓	✓	✓	✓	✓	✓	×	×	×	×	✓	✓	✓	×	✓
[39]	✓	✓	×	✓	✓	×	×	×	×	×	×	×	✓	×	✓
The proposed model	✓	✓	✓	✓	✓	✓	✓	✓	✓	✓	✓	✓	✓	✓	✓

incorporate CCHP, HRSs, RCSs, and FCETs to achieve enhanced resilience in the seaport PDN.
- A scenario-based optimization formulation is developed in the form of a mixed-integer nonlinear programming (MINLP) problem, which is then linearized into a mixed-integer linear programming (MILP) model using linearization techniques.

The rest of the paper is structured as follows. The detailed modelling of the proposed integrated seaport multi-energy system is provided in Section 2. The proposed model is tested and numerically analyzed on the IEEE 33-node test system in Section 3. The paper is concluded in Section 4.

2 | AN INTEGRATED SEAPORT MULTI-ENERGY SYSTEM FRAMEWORK: MODELS

2.1 | Proposed framework

This paper proposes a framework for the deployment of hydrogen-based microgrids integrated with the CCHP system in seaports to enhance energy resilience and reduce carbon emissions. The HRS is assumed to be built on the traditional petroleum refueling stations of the public transportation operation center to make it economically feasible. The HRS utilizes renewable energy resources such as photovoltaic and wind power to generate "green hydrogen", and it also enters into hydrogen supply agreements with industrial firms that generate purified hydrogen (PH) from industrial by-products, known as "blue hydrogen". The hydrogen is further stored in tanks and sold to private hydrogen-powered vehicles and FCETs. The FCETs have scheduled travel paths and can be rapidly deployed to reach the neighbouring V2G node when disasters happen. RCSs are able to rapidly isolate the damaged lines allowing the network reconfiguration. The coordination of network reconfiguration with the energy scheduling of hydrogen-based microgrids is an effective way to improve the survivability of critical loads during emergencies.

The operation of the CCHP system involves utilizing natural gas as a source for generating both power and heat. The heat recovery boiler captures the excess heat generated during this process, which can then be used to produce cooling energy through an absorption chiller (AC). Additionally, since CCHP systems are able to produce electricity on-site, they can reduce the need for energy transmission and distribution, which can lead to a reduction in energy losses and greenhouse gas emissions. Furthermore, CCHP systems can increase energy security and resilience by providing a reliable source of electricity and thermal energy, even during power outages or other disruptions to the grid. The conceptual architecture of the low-carbon hydrogen-based seaport multi-energy system is shown in Figure 2, which includes the natural-gas-powered CCHP system, the renewable-powered HRSs, optimal grid reconfiguration via RCSs, centralized scheduling system of FCETs, and hydrogen-aided on-emergency FCET dispatch system. The detailed modelling of each energy infrastructure is provided in subsequent sections.

2.2 | Objective function

The goal of the proposed objective function (1a) is to minimize the capital investment cost, the annualized operation cost in normal operation scenarios, and the annualized unserved energy penalty cost under contingency scenarios from the perspective of the private seaport owner. Note that, the seaport owner is able to make decisions on the purchase of HRSs/RESs/FCETs/RCSs as well as where to locate these facilities. The commercial seaport is committed to supplying energy to the users who are supported by the port, independent of port ownership. Failure to meet the energy demand will result in penalty costs for the port owner [5]. The capital investment cost term IC stipulates the investment decisions on the installation of HRSs/RESs/RCSs and the FCETs purchase, which are evaluated via the investment cost factor (ϑ), as shown in Equation (1b). ϱ represents the total number of days in the planning horizon. The occurrence of normal/contingency operation scenarios is represented by $\mathcal{P}^{\mathrm{n}}/\mathcal{P}^{\mathrm{c}}$, i.e. normal operation scenarios constitute 98% of the scheduled horizon. $\mathrm{OPE}^{\mathrm{n}}$ and $\mathrm{OPE}^{\mathrm{c}}$ represent the daily operation cost with respect to the normal/contingency operation terms.

$$\min \mathrm{IC} + \varrho \mathcal{P}^{\mathrm{n}} \mathrm{OPE}^{\mathrm{n}} + \varrho \mathcal{P}^{\mathrm{c}} \mathrm{OPE}^{\mathrm{c}} \tag{1a}$$

$$\begin{aligned} \mathrm{IC} = & \sum_{i \in \mathbf{N}^{\mathrm{hrs}}} \vartheta^{\mathrm{hrs}} z_i + \sum_{i \in \mathbf{N}^{\mathrm{hrs}}} \sum_{k \in \mathbf{K}} \vartheta_k^{\mathrm{res}} \varkappa_{k,i}^{\mathrm{res}} \overline{P}_k^{\mathrm{res}} \\ & + \sum_{i \in \mathbf{N}^{\mathrm{hrs}}} \left(\vartheta^{\mathrm{p2h}} G_i^{\mathrm{U}} + \vartheta^{\mathrm{ht}} \mathrm{SH}_i^{\mathrm{U}} + \vartheta^{\mathrm{fc}} \mathrm{FC}_i^{\mathrm{U}} \right) \\ & + \sum_{l \in \mathbf{L}} \vartheta^{\mathrm{sw}} \left(s_l^{\mathrm{U}} + s_l^{\mathrm{D}} \right) + \sum_{m \in \mathbf{M}} \vartheta^{\mathrm{et}} y_m \end{aligned} \tag{1b}$$

Constraint (1c) represents the expected daily operation cost of the system under normal operating conditions and consists of the probability of each normal operation scenario multiplied by the daily operation and maintenance costs for RESs/HRSs/FCETs with cost coefficient ($\varkappa$), the daily amount of purchased electricity/natural gas/purified by-product hydrogen, and the amount of hydrogen sold to local users with the price coefficient (λ). Constraint (1d) highlights the expected daily operation cost of the system under emergency scenarios and is characterized by the summation of the penalty costs of unserved power/heating/cooling demand over the entire contingency scenarios.

$$\begin{aligned} \mathrm{OPE}^{\mathrm{n}} = & \sum_{w \in \mathbf{\Omega}} \mathcal{P}_w \Bigg(\sum_{t \in \mathbf{T}^n} \Bigg(\sum_{i \in \mathbf{N}^{hrs}} \sum_{k \in \mathbf{K}} \varkappa_{k,t}^{\mathrm{res}} \varkappa_{k,i}^{\mathrm{res}} \overline{P}_k^{\mathrm{res}} \\ & + \sum_{i \in \mathbf{N}^{\mathrm{hrs}}} \left(\varkappa_t^{\mathrm{p2h}} G_i^{\mathrm{U}} + \varkappa_t^{\mathrm{ht}} \mathrm{SH}_i^{\mathrm{U}} + \varkappa_t^{\mathrm{fc}} \mathrm{FC}_i^{\mathrm{U}} \right) \end{aligned}$$

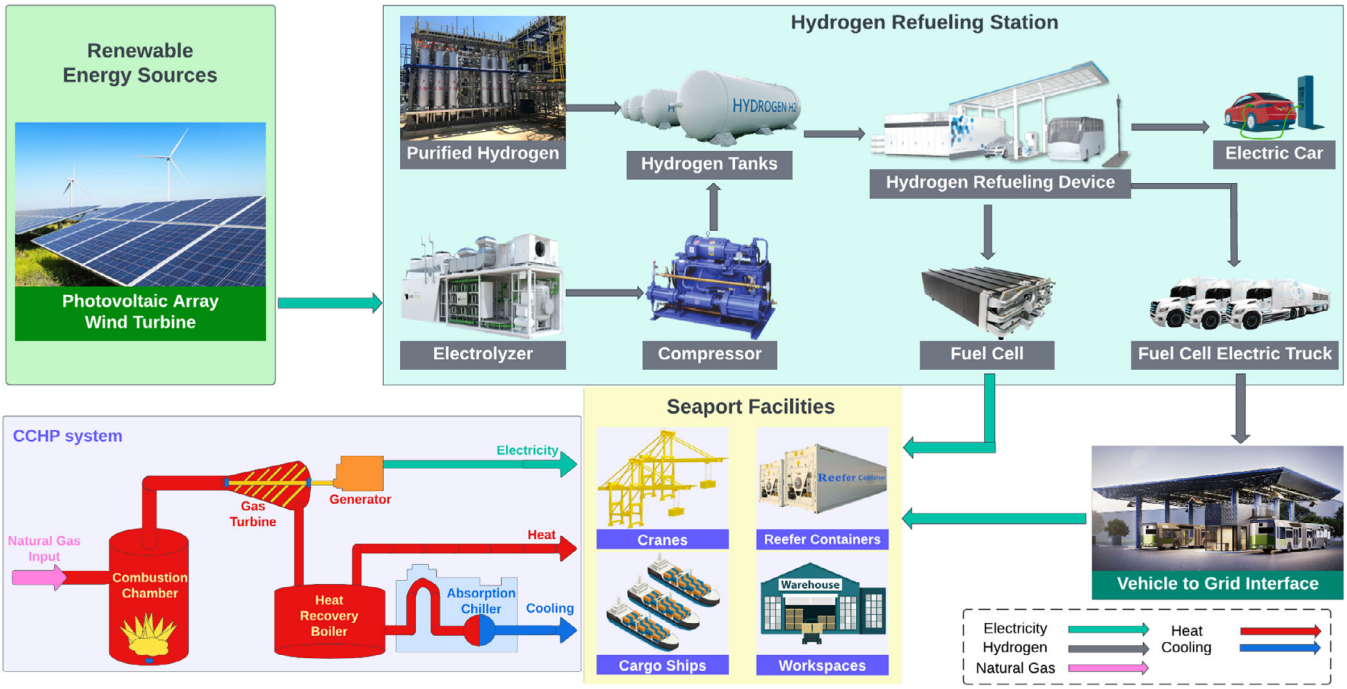

FIGURE 2 The proposed integrated seaport multi-energy system: the Big Picture.

$$+\sum_{i\in\mathbf{N}^{\text{sub}}}\lambda^{\text{grid}}_{w,t}P^{\text{sub}}_{w,i,t}+\lambda^{\text{gas}}_{w}G_{w,t}+\sum_{m\in\mathbf{M}}\varkappa^{\text{et}}_{m,t}y_m$$

$$+\sum_{i\in\mathbf{N}^{\text{hrs}}}\left(\lambda^{\text{ph}}g^{\text{ph}}_{w,i,t}-\lambda^{\text{h}}g^{\text{sh}}_{w,i,t}\right)\Big)\Big) \tag{1c}$$

$$\text{OPE}^{\text{c}}=\sum_{\varepsilon\in\Xi}\mathcal{P}'_{\varepsilon}\sum_{i\in\mathbf{N}}\sum_{t\in\mathbf{T}^{\text{c}}_{\varepsilon}}\lambda^{\text{UD}}(P^{\text{UD}}_{\varepsilon,i,t}+H^{\text{UD}}_{\varepsilon,t}+C^{\text{UD}}_{\varepsilon,t}) \tag{1d}$$

The detailed modelling of each aforementioned decision variable is presented in Sections 2.3 to 2.5. In our work, we incorporate both planning and operational aspects to provide a comprehensive solution. The first stage (Section 2.3) focuses on planning, wherein decisions are made in collaboration with the operational aspects addressed in the second stage (Section 2.4 and 2.5). This dual-stage approach determines the capacity and location of various technologies such as FCETs, RESs, HRSs, and RCSs under different operational conditions. Subsequently, the second stage contains both normal and contingency operational scenarios to validate the robustness of the planning decisions made in the first stage.

2.3 | Planning constraints

Initially, HRSs will serve hydrogen vehicles in nearby areas and will be deployed at candidate nodes $\mathbf{N}^{\text{hrs}}$ with petroleum refueling capability. We divide the port into several areas, denoted by o, according to the different services that the port can provide, such as cold chain transportation, port logistics, warehouses etc. To meet the hydrogen consumption requirements in every region $o\in\mathbf{\Gamma}$, it is essential to have at least one HRS located in that area, as enforced in Equation (2a). Constraint (2b) limits the total number of installed HRSs not to exceed a certain threshold due to urban planning and capital expenditure restrictions. The installed capacity for P2H facilities, HT, RES type k, and on-site FC at HRS candidate node i is dependent on the installation decision of HRSs, as constrained in Equations (2c)–(2f), respectively. The total number of RCSs that can be installed is represented by constraint (2g). The maximum number of FCETs that can be purchased is constrained by Equation (2h). It is worth mentioning that V2G interfaces are assumed to be pre-installed at all HRS candidate nodes.

$$\sum_{i\in\mathbf{N}^{\text{hrs}}_{o}}z_i\geq 1 \qquad o\in\mathbf{\Gamma} \tag{2a}$$

$$\sum_{i\in\mathbf{N}^{\text{hrs}}}z_i\leq\overline{N}^{\text{hrs}} \tag{2b}$$

$$\underline{P}^{\text{p2h}}z_i\leq G^{\text{U}}_i\leq\overline{P}^{\text{p2h}}z_i \qquad i\in\mathbf{N}^{\text{hrs}} \tag{2c}$$

$$\underline{\text{SH}}z_i\leq\text{SH}^{U}_i\leq\overline{\text{SH}}z_i \qquad i\in\mathbf{N}^{\text{hrs}} \tag{2d}$$

$$0\leq\varkappa^{\text{res}}_{k,i}\leq X^{\text{res}}_{k}z_i \qquad k\in\mathbf{K},\, i\in\mathbf{N}^{\text{hrs}} \tag{2e}$$

$$\underline{\text{FC}}z_i\leq\text{FC}^{\text{U}}_i\leq\overline{\text{FC}}z_i \qquad i\in\mathbf{N}^{\text{hrs}} \tag{2f}$$

$$\sum_{l\in\mathbf{L}}\left(s^{\text{U}}_l+s^{\text{D}}_l\right)\leq\overline{N}^{\text{rcs}} \tag{2g}$$

$$\sum_{m\in\mathbf{M}}y_m\leq\overline{N}^{\text{et}} \tag{2h}$$

2.4 | Normal operation constraints

Hydrogen inflow of HRSs, as characterized in Equation (3a), comprises two parts: 1) the amount of renewable-energy-powered electrolyzer produced hydrogen (as in Equations (3b)–(3d)), and 2) purchased purified by-product hydrogen (as in Equations (3e) and (3f)). Constraint (3b) regulates that the power output of RESs is the power input of the P2H system. Constraint (3c) shows that the power consumed by the P2H system is limited by the installed capacity. The maximum power generation from RES type k at time t is restricted by both the hourly renewable power generation factor under different scenarios and the number of RES type k installed in the HRS at candidate node i, as in Equation (3d). Daily available PH that can be purchased is limited by constraint (3e). The maximum daily hydrogen inflow for each HRS is restricted by constraint (3f). Constraints (3g)–(3i) are to restrict the retail hydrogen selling of HRSs. The HT's storage level inside the installed HRS is defined by Equations (3j)–(3l).

$$\forall\{w \in \mathbf{\Omega}, i \in \mathbf{N}^{\mathrm{hrs}}, t \in \mathbf{T}^{\mathrm{n}}\}$$

$$\mathrm{HF}_{w,i,t} = \eta^{\mathrm{p2h}}\sigma^{\mathrm{p2h}}P^{\mathrm{p2h}}_{w,i,t} + g^{\mathrm{ph}}_{w,i,t} \tag{3a}$$

$$P^{\mathrm{p2h}}_{w,i,t} = \sum_{k\in\mathbf{K}} P^{\mathrm{res}}_{w,k,i,t} \tag{3b}$$

$$0 \le P^{\mathrm{p2h}}_{w,i,t} \le G^{\mathrm{U}}_{i} \tag{3c}$$

$$0 \le P^{\mathrm{res}}_{w,k,i,t} \le \psi^{\mathrm{res}}_{w,k,t}\overline{P}^{\mathrm{res}}_{k}\, x^{\mathrm{res}}_{k,i} \qquad k \in \mathbf{K} \tag{3d}$$

$$0 \le \sum_{t\in\mathbf{T}^{\mathrm{n}}} g^{\mathrm{ph}}_{w,i,t} \le \overline{\mathrm{PH}}z_i \tag{3e}$$

$$\sum_{t\in\mathbf{T}^{\mathrm{n}}} \mathrm{HF}_{w,i,t} \le \overline{g}^{\mathrm{hrs}}_{i} \tag{3f}$$

$$0 \le g^{\mathrm{sh}}_{w,i,t} \le \rho_{w,i,t} g^{\mathrm{D}}_{w,o,t} \qquad o \in \mathbf{\Gamma}, i \in \mathbf{N}^{\mathrm{hrs}}_{o} \tag{3g}$$

$$\sum_{i\in\mathbf{N}^{\mathrm{hrs}}_{o}} \rho_{w,i,t} = 1 \qquad o \in \mathbf{\Gamma} \tag{3h}$$

$$\rho_{w,i,t} \le z_i \qquad o \in \mathbf{\Gamma}, i \in \mathbf{N}^{\mathrm{hrs}}_{o} \tag{3i}$$

$$\mathrm{SH}_{w,i,t} = \mathrm{SH}_{i,t-1} + \mathrm{HF}_{w,i,t} - g^{\mathrm{sh}}_{w,i,t} - g^{\mathrm{hrs}}_{w,i,t} \qquad t \ge 2 \tag{3j}$$

$$\mathrm{SH}_{w,i,t} = \mathrm{HF}_{w,i,t} - g^{\mathrm{sh}}_{w,i,t} - g^{\mathrm{hrs}}_{w,i,t} \qquad t = 1 \tag{3k}$$

$$0 \le \mathrm{SH}_{w,i,t} \le \mathrm{SH}^{\mathrm{U}}_{i} \tag{3l}$$

Based on the CCHP system configuration, as shown in Figure 2, the power output of the CCHP system is only supplied by the GT—see constraint (4a). Similarly, the heating output of the CCHP system is solely provided by GT's heating generation—see constraint (4b), wherein variable $\alpha_{w,t} \in [0, 1]$ stipulates the ratio of GT's heating generation to use for CCHP system's heating output under contingency scenario w. The remaining heating generation of GT is utilized for AC refrigeration, which is the only cooling source of the CCHP system—see constraint (4c). Limitations on the purchased natural gas as well as the power, heating, and cooling output of the CCHP system are represented by constraints (4d)–(4g).

$$\forall\{w \in \mathbf{\Omega}, i \in \mathbf{N}^{\mathrm{gt}}, t \in \mathbf{T}^{\mathrm{n}}\}$$

$$P^{t}_{w,i,t} = \beta^{\mathrm{gt,e}} CG_{w,t} \tag{4a}$$

$$H^{t}_{w,t} = \alpha_{w,t}\beta^{\mathrm{gt,h}} CG_{w,t} \tag{4b}$$

$$C^{t}_{w,t} = \beta^{\mathrm{ac}}\left[(1-\alpha_{w,t})\beta^{\mathrm{gt,h}} CG_{w,t}\right] \tag{4c}$$

$$0 \le G_{w,t} \le \overline{G} \tag{4d}$$

$$0 \le P^{t}_{w,i,t} \le \overline{P^{t}} \tag{4e}$$

$$0 \le H^{t}_{w,t} \le \overline{H^{t}} \tag{4f}$$

$$0 \le C^{t}_{w,t} \le \overline{C^{t}} \tag{4g}$$

The variations in the SOC of the HS over time are determined by its charging and discharging behaviours, as denoted in constraints (5a) and (5b). Constraints (5c) and (5d) restrict the HS's heat charging and discharging capacities, respectively. Constraint (5e) indicates that HS's charging and discharging are mutually exclusive. Constraint (5f) enforces a boundary for the SOC of the HS. Constraint (5g) ensures that there will be at least $S^{\mathrm{hs},ini}$ amount of energy stored in HS for use in the next operation day.

$$\forall\{w \in \mathbf{\Omega}, t \in \mathbf{T}^{\mathrm{n}}\}$$

$$S^{\mathrm{hs}}_{w,t} = (1-\gamma)S^{\mathrm{hs}}_{w,t-1} + \left(H^{\mathrm{hs,c}}_{w,t}\eta^{\mathrm{hs,c}} - \frac{H^{\mathrm{hs,d}}_{w,t}}{\eta^{\mathrm{hs,d}}}\right) t \ge 2 \tag{5a}$$

$$S^{\mathrm{hs}}_{w,t} = S^{\mathrm{hs,ini}} + \left(H^{\mathrm{hs,c}}_{w,t}\eta^{\mathrm{hs,c}} - \frac{H^{\mathrm{hs,d}}_{w,t}}{\eta^{\mathrm{hs,d}}}\right) \qquad t = 1 \tag{5b}$$

$$0 \le H^{\mathrm{hs,c}}_{w,t} \le \overline{H^{\mathrm{hs,c}}}\mu^{\mathrm{hs,c}}_{w,t} \tag{5c}$$

$$0 \le H^{\mathrm{hs,d}}_{w,t} \le \overline{H^{\mathrm{hs,d}}}\mu^{\mathrm{hs,d}}_{w,t} \tag{5d}$$

$$\mu^{\mathrm{hs},c}_{w,t} + \mu^{\mathrm{hs,d}}_{w,t} \le 1 \tag{5e}$$

$$\underline{S^{\mathrm{hs}}} \le S^{\mathrm{hs}}_{w,t} \le \overline{S^{\mathrm{hs}}} \tag{5f}$$

$$S^{\mathrm{hs}}_{w,t} = S^{\mathrm{hs,ini}} \qquad t = 24 \tag{5g}$$

Constraints (6a) and (6b) respectively represent the heating and cooling energy balance in the seaport system. In addition to the cooling output of the CCHP system, EC also supplies cooling energy to satisfy the cooling demand in the seaport system. The relationships between the real and reactive power in the CCHP system are described in constraint (6c). The power consumption of the EC is restricted by Equation (6d).

$$\forall\{w \in \mathbf{\Omega}, g \in \mathbf{N}^{\mathrm{gt}}, e \in \mathbf{N}^{\mathrm{ec}}, t \in \mathbf{T}^{\mathrm{n}}\}$$

$$H^{t}_{w,t} + H^{\mathrm{hs,d}}_{w,t} - H^{\mathrm{hs,c}}_{w,t} = H^{\mathrm{D}}_{w,t} \tag{6a}$$

$$C^{t}_{w,t} + \beta^{ec} P^{ec}_{w,e,t} = C^{D}_{w,t} \tag{6b}$$

$$Q^{t}_{w,g,t} = \delta^{t} P^{t}_{w,g,t} \tag{6c}$$

$$0 \le P^{ec}_{w,e,t} \le \overline{P^{ec}} \tag{6d}$$

Nodal power balance constraints (7a) and (7b) and power flow constraint (7c) are modelled based on the linearized DistFlow model [40]. Note that, notations $i(l)$ and $j(l)$ represent, respectively, the sending and receiving terminals of the overhead power distribution line l. The squared voltage level at each node is denoted as $V_{w,i,t}$, which ranges within $((1 \pm 0.05)V_{base})^2$; V_{base} is the base voltage of the grid.

$$\forall\{w \in \mathbf{\Omega}, i \in \mathbf{N}, t \in \mathbf{T}^{n}\}$$

$$\begin{aligned}
&\sum_{l \in \mathbf{L}: i(l)=i} P^{f}_{w,l,t} - \sum_{l \in \mathbf{L}: j(l)=i} P^{f}_{w,l,t} = \sum_{s \in \mathbf{N}^{sub}: s=i} P^{sub}_{w,s,t} \\
&+ \sum_{h \in \mathbf{N}^{hrs}: h=i} P^{hrs}_{w,h,t} + \sum_{g \in \mathbf{N}^{gt}: g=i} P^{t}_{w,g,t} - P^{D}_{w,i,t} \\
&- \sum_{e \in \mathbf{N}^{ec}: e=i} P^{ec}_{w,e,t}
\end{aligned} \tag{7a}$$

$$\begin{aligned}
&\sum_{l \in \mathbf{L}: i(l)=i} Q^{f}_{w,l,t} - \sum_{l \in \mathbf{L}: j(l)=i} Q^{f}_{w,l,t} = \sum_{s \in \mathbf{N}^{sub}: s=i} Q^{sub}_{w,s,t} \\
&+ \sum_{g \in \mathbf{N}^{gt}: g=i} Q^{t}_{w,g,t} - Q^{D}_{w,i,t}
\end{aligned} \tag{7b}$$

$$V_{w,i(l),t} - V_{w,j(l),t} = 2\left(P^{f}_{w,l,t} r_l + Q^{f}_{w,l,t} x_l\right) \tag{7c}$$

Active/reactive power output from the upstream grid to the seaport system is constrained as Equations (8a) and (8b). Constraint (8c) represents the active power generated by the on-site FC inside the HRS. The branch flow is constrained by Equations (8d) and (8e).

$$\forall\{w \in \mathbf{\Omega}, , s \in \mathbf{N}^{sub}, h \in \mathbf{N}^{hrs}, l \in \mathbf{L}, t \in \mathbf{T}^{n}\}$$

$$0 \le P^{sub}_{w,s,t} \le \overline{P}^{sub} \tag{8a}$$

$$-\overline{P}^{sub} \delta^{sub} \le Q^{sub}_{w,s,t} \le \overline{P}^{sub} \delta^{sub} \tag{8b}$$

$$0 \le P^{hrs}_{w,h,t} = \eta^{fc} \sigma^{fc} g^{hrs}_{w,h,t} \le FC^{U}_{h} \tag{8c}$$

$$-\overline{P}^{f}_{l} \le P^{f}_{w,l,t} \le \overline{P}^{f}_{l} \tag{8d}$$

$$-\overline{Q}^{f}_{l} \le Q^{f}_{w,l,t} \le \overline{Q}^{f}_{l} \tag{8e}$$

2.5 | Contingency operation constraints

If a catastrophe occurs, overhead branches within the seaport PDN may be damaged, leading to potential emergency load shedding in order to maintain the system's security. To minimize the economic losses and ensure a timely response, it is essential to dispatch FCETs that are pre-located at depots and utilize their hydrogen storage via V2G interfaces during the contingency period. Note that the terms τ^{s}_{ε} and τ^{e}_{ε} inside the set $\mathbf{T}^{c}_{\varepsilon}$ respectively represent the starting and ending time of the contingency scenario ε. One can notice that constraints (9a)–(12d) for contingency operation modelling share similarities with those presented for the normal operation modelling. However, the contingency operation model employs a distinct set of decision variables, denoted by a prime superscript.

Under contingency operation, the hydrogen inflow of HRSs is subject to the constraint introduced in Equation (9a). Furthermore, constraint (9b) mandates that all power output from RESs must serve as the input for the P2H system. Constraint (9c) governs the power consumption of the P2H system by the installed capacity. Both the hourly renewable power generation factor under different scenarios and the number of installed RES units of type k at candidate node i restrict the maximum power generation from RES type k at time t, as indicated in Equation (9d). Constraint (9e) imposes a limit on the daily available PH that can be purchased. Constraint (9f) restricts the maximum daily hydrogen inflow for each HRS. The storage level of HT in the installed HRS is determined by constraints (9g)–(9i). It is worth noting that the selling of hydrogen to local users is halted during contingencies to utilize all the purchased PH as well as hydrogen generated from HRS for load supply via the on-site FC.

$$\forall\left\{\varepsilon \in \Xi, i \in \mathbf{N}^{hrs}, t \in \mathbf{T}^{c}_{\varepsilon} : \left[\tau^{s}_{\varepsilon}, \tau^{e}_{\varepsilon}\right]\right\}$$

$$HF'_{\varepsilon,i,t} = \eta^{p2h} \sigma^{p2h} P'^{p2h}_{\varepsilon,i,t} + g'^{ph}_{\varepsilon,i,t} \tag{9a}$$

$$P'^{p2h}_{\varepsilon,i,t} = \sum_{k \in \mathbf{K}} P'^{res}_{\varepsilon,k,i,t} \tag{9b}$$

$$0 \le P'^{p2h}_{\varepsilon,i,t} \le G^{U}_{i} \tag{9c}$$

$$0 \le P'^{res}_{\varepsilon,k,i,t} \le \psi'^{res}_{\varepsilon,k,t} \overline{P}^{res}_{k} x^{res}_{k,i} \qquad k \in \mathbf{K} \tag{9d}$$

$$0 \le \sum_{t \in \mathbf{T}^{c}_{\varepsilon}} g'^{ph}_{\varepsilon,i,t} \le \overline{PH} \tilde{x}_i \tag{9e}$$

$$\sum_{t \in \mathbf{T}^{c}_{\varepsilon}} HF'_{\varepsilon,i,t} \le \overline{g}^{hrs}_{i} \tag{9f}$$

$$SH'_{\varepsilon,i,t} = SH'_{\varepsilon,i,t-1} + HF'_{\varepsilon,i,t} - g'^{hrs}_{\varepsilon,i,t} \qquad t \ne \tau^{s}_{\varepsilon} \tag{9g}$$

$$SH'_{\varepsilon,i,t} = HF'_{\varepsilon,i,t} - g'^{hrs}_{\varepsilon,i,t} \qquad t = \tau^{s}_{\varepsilon} \tag{9h}$$

$$0 \le SH'_{\varepsilon,i,t} \le SH^{U}_{i} \tag{9i}$$

The CCHP operation constraints during contingency scenarios are very similar to those during normal operation. Note that, the operation of CCHP under a contingency scenario is here based on an assumption that the natural gas network is not affected by the extreme event. As a result, CCHP can continuously supply heating and cooling energy to the system. The output power, heating, and cooling, as well as the natural gas

consumption by CCHP, are defined in Equations (10a)–(10g).

$$\forall\{\varepsilon \in \Xi, i \in \mathbf{N}^{\mathrm{gt}}, t \in \mathbf{T}_{\varepsilon}^{\mathrm{c}} : [\tau_{\varepsilon}^{\mathrm{s}}, \tau_{\varepsilon}^{\mathrm{e}}]\}$$

$$P_{\varepsilon,i,t}^{\prime \iota} = \beta^{\mathrm{gt,e}} \mathcal{C} G_{\varepsilon,t}^{\prime} \tag{10a}$$

$$H_{\varepsilon,t}^{\prime \iota} = \alpha_{\varepsilon,t}^{\prime} \beta^{\mathrm{gt,h}} \mathcal{C} G_{\varepsilon,t}^{\prime} \tag{10b}$$

$$C_{\varepsilon,t}^{\prime \iota} = \beta^{\mathrm{ac}} \left[(1 - \alpha_{\varepsilon,t}^{\prime}) \beta^{\mathrm{gt,h}} \mathcal{C} G_{\varepsilon,t}^{\prime} \right] \tag{10c}$$

$$0 \le G_{\varepsilon,t}^{\prime} \le \overline{G} \tag{10d}$$

$$0 \le P_{\varepsilon,i,t}^{\prime \iota} \le \overline{P^{\iota}} \tag{10e}$$

$$0 \le H_{\varepsilon,t}^{\prime \iota} \le \overline{H^{\iota}} \tag{10f}$$

$$0 \le C_{\varepsilon,t}^{\prime \iota} \le \overline{C^{\iota}} \tag{10g}$$

Constraints (11a)–(11f) govern the energy level of HS and control the charging and discharging status of HS.

$$\forall\{\varepsilon \in \Xi, t \in \mathbf{T}_{\varepsilon}^{\mathrm{c}} : [\tau_{\varepsilon}^{\mathrm{s}}, \tau_{\varepsilon}^{\mathrm{e}}]\}$$

$$S_{\varepsilon,t}^{\prime \mathrm{hs}} = (1 - \gamma) S_{\varepsilon,t-1}^{\prime \mathrm{hs}} + \left(H_{\varepsilon,t}^{\prime \mathrm{hs},c} \eta^{\mathrm{hs,c}} - \frac{H_{\varepsilon,t}^{\prime \mathrm{hs},d}}{\eta^{\mathrm{hs},d}} \right) t \ne \tau_{\varepsilon}^{\mathrm{s}} \tag{11a}$$

$$S_{\varepsilon,t}^{\prime \mathrm{hs}} = S^{\mathrm{hs,ini}} + \left(H_{\varepsilon,t}^{\prime \mathrm{hs},c} \eta^{\mathrm{hs,c}} - \frac{H_{\varepsilon,t}^{\prime \mathrm{hs},d}}{\eta^{\mathrm{hs},d}} \right) t = \tau_{\varepsilon}^{\mathrm{s}} \tag{11b}$$

$$0 \le H_{\varepsilon,t}^{\prime \mathrm{hs,c}} \le \overline{H^{\mathrm{hs},c}} \mu_{\varepsilon,t}^{\prime \mathrm{hs,c}} \tag{11c}$$

$$0 \le H_{\varepsilon,t}^{\prime \mathrm{hs,d}} \le \overline{H^{\mathrm{hs},d}} \mu_{\varepsilon,t}^{\prime \mathrm{hs,d}} \tag{11d}$$

$$\mu_{\varepsilon,t}^{\prime \mathrm{hs,c}} + \mu_{\varepsilon,t}^{\prime \mathrm{hs,d}} \le 1 \tag{11e}$$

$$\underline{S^{\mathrm{hs}}} \le S_{\varepsilon,t}^{\prime \mathrm{hs}} \le \overline{S^{\mathrm{hs}}} \tag{11f}$$

It is worth mentioning that the cooling energy supply from the EC may be interrupted in case the branch is damaged or the node with EC equipment is isolated due to RCS operation. The CCHP heating/cooling energy balance constraints, (12a)–(12b), have been modified to include two new variables, $H_{\varepsilon,t}^{\mathrm{UD}}$ and $C_{\varepsilon,t}^{\mathrm{UD}}$, which indicate the unserved heating/cooling demand at the restoration time step t during the contingency operation scenario ε. Constraint (12c) enforces the relationship between the active and reactive power generation of the CCHP. Additionally, constraint (12d) ensures that the EC can only function when the node is energized.

$$\forall\{\varepsilon \in \Xi, g \in \mathbf{N}^{\mathrm{gt}}, e \in \mathbf{N}^{\mathrm{ec}}, t \in \mathbf{T}_{\varepsilon}^{\mathrm{c}} : [\tau_{\varepsilon}^{\mathrm{s}}, \tau_{\varepsilon}^{\mathrm{e}}]\}$$

$$H_{\varepsilon,t}^{\prime \iota} + H_{\varepsilon,t}^{\prime \mathrm{hs,d}} + H_{\varepsilon,t}^{\mathrm{UD}} - H_{\varepsilon,t}^{\prime \mathrm{hs,c}} = H_{\varepsilon,t}^{\prime \mathrm{D}} \tag{12a}$$

$$C_{\varepsilon,t}^{\prime \iota} + \beta^{\mathrm{ec}} P_{\varepsilon,e,t}^{\prime \mathrm{ec}} + C_{\varepsilon,t}^{\mathrm{UD}} = C_{\varepsilon,t}^{\prime \mathrm{D}} \tag{12b}$$

$$Q_{\varepsilon,g,t}^{\prime \iota} = \delta^{\iota} P_{\varepsilon,g,t}^{\prime \iota} \tag{12c}$$

$$0 \le P_{\varepsilon,e,t}^{\prime \mathrm{ec}} \le \overline{P^{\mathrm{ec}}} (1 - d_{\varepsilon,e,t}^{\mathrm{N}}) \tag{12d}$$

The power output of FCET m is constrained in Equations (13a) and (13b). The transportation status for each FCET m is constrained in Equations (13c)–(13g). The condition for FCET m to stay at node i is defined by Equation (13c) whether FCET m arrives at node i at the current time step t or has already arrived at one of the previous time steps. Constraint (13d) represents that the arrival time of FCET $x_{\varepsilon,i,m,t}^{\mathrm{et,a}}$ is determined by the decision on its travel $x_{\varepsilon,i,m}^{\mathrm{et,g}}$ and the duration of the trip $\mathrm{TR}_{i,m}$. Note that, the symbol $\Theta_{\varepsilon,t}$ represents the position of the current time t within the entire disaster cycle c during the restoration stage. For instance, the duration of contingency scenario $\varepsilon = 1$ is defined as $t \in \mathbf{T}_1^{\mathrm{c}} : \{7, 8, 9, 10, 11, 12\}$, where $\Theta_{1,8} = 2$ shows that $t = 8$ is the second time step within the entire restoration stage. If FCET m is decided to travel to node i while initially at a distance from the node, its on-the-way behaviour is defined as Equation (13e). The travel behaviour of FCET m is restricted by the purchase decision for each FCET m and the maximum parking limitation at node i, as enforced in Equations (13f) and (13g). FCET's HT storage level is defined in Equations (13h)–(13j). The FCET's hydrogen consumption comes from either the FCET traveling to an HRS candidate node, or connected with the V2G interface to produce power, as shown in Equations (13h) and (13i). It is worth mentioning that the FCET fleets are only used as an emergency power backup, and the initial hydrogen storage level of each FCET is assumed to be full and prepared for contingency events. The storage level of HT inside FCETs is limited by the purchase decision y_m and the capacity $\underline{E}/\overline{E}$, as enforced in Equation (13j).

$$\forall\{\varepsilon \in \Xi, i \in \mathbf{N}^{\mathrm{hrs}}, m \in \mathbf{M}, t \in \mathbf{T}_{\varepsilon}^{\mathrm{c}} : [\tau_{\varepsilon}^{\mathrm{s}}, \tau_{\varepsilon}^{\mathrm{e}}]\}$$

$$0 \le P_{\varepsilon,i,m,t}^{\mathrm{et}} = \eta^{\mathrm{et}} \sigma^{\mathrm{et}} g_{\varepsilon,i,m,t}^{\mathrm{et}} \le \overline{P}_{m}^{\mathrm{et}} x_{\varepsilon,i,m,t}^{\mathrm{et,s}} \tag{13a}$$

$$\sum_{m \in \mathbf{M}} P_{\varepsilon,i,m,t}^{\mathrm{et}} \le \overline{P}^{\mathrm{v2g}} \tag{13b}$$

$$x_{\varepsilon,i,m,t}^{\mathrm{et,s}} = \sum_{t=\tau_{\varepsilon}^{s}}^{t} x_{\varepsilon,i,m,t}^{\mathrm{et,a}} \tag{13c}$$

$$\sum_{t \in \mathbf{T}_{\varepsilon}^{\mathrm{c}}} \Theta_{\varepsilon,t} x_{\varepsilon,i,m,t}^{\mathrm{et,a}} = \mathrm{TR}_{i,m} x_{\varepsilon,i,m}^{\mathrm{et,g}} \tag{13d}$$

$$x_{\varepsilon,i,m,t}^{\mathrm{et,o}} = x_{\varepsilon,i,m}^{\mathrm{et,g}} - x_{\varepsilon,i,m,t}^{\mathrm{et,s}} \tag{13e}$$

$$\sum_{i \in \mathbf{N}^{\mathrm{hrs}}} x_{\varepsilon,i,m}^{\mathrm{et,g}} \le y_m \tag{13f}$$

$$\sum_{m \in \mathbf{M}} x_{\varepsilon,i,m}^{\mathrm{et,g}} \le \overline{N}_{i}^{\mathrm{park}} \tag{13g}$$

$$E_{\varepsilon,m,t} = E_{\varepsilon,m,t-1} - \sum_{i \in \mathbf{N}^{\mathrm{hrs}}} \mathrm{TH}_{m} x_{\varepsilon,i,m,t}^{\mathrm{et,o}} - \sum_{i \in \mathbf{N}^{\mathrm{hrs}}} g_{\varepsilon,i,m,t}^{\mathrm{et}} t \ne \tau_{\varepsilon}^{\mathrm{s}} \tag{13h}$$

$$E_{\varepsilon,m,t} = \overline{E} y_m - \sum_{i \in \mathbf{N}^{\mathrm{hrs}}} \mathrm{TH}_{m} x_{\varepsilon,i,m,t}^{\mathrm{et,o}} - \sum_{i \in \mathbf{N}^{\mathrm{hrs}}} g_{\varepsilon,i,m,t}^{\mathrm{et}} t = \tau_{\varepsilon}^{\mathrm{s}} \tag{13i}$$

$$\underline{E} y_m \le E_{\varepsilon,m,t} \le \overline{E} y_m \tag{13j}$$

Constraints (14a) and (14b) represent the nodal power balance equations. The contingency scenarios have an initial condition assuming that the branch connecting the seaport to the upstream grid is damaged, resulting in no power flowing into the seaport PDN from the upstream grid. The terms $P^{\mathrm{UD}}_{\varepsilon,i,t}$ and $Q^{\mathrm{UD}}_{\varepsilon,i,t}$ are added to the power balance equations to indicate the unserved active and reactive power demand of each node i at time t under contingency scenario ε. Big-M method [41] is applied to the nodal voltage constraints (14c) and (14d), which ensures that these constraints are only active when the distribution line l is energized. Note that, the squared voltage level at each node during contingencies is denoted as $V'_{\varepsilon,i,t}$, ranging within $((1 \pm 0.05)V_{\mathrm{base}})^2$. Constraint (14e) ensures that node i is deactivated in case of an outage emergency.

$$\forall\{\varepsilon \in \Xi, n \in \mathbf{N}, l \in \mathbf{L}, t \in \mathbf{T}^{\mathrm{c}}_{\varepsilon} : [\tau^{\mathrm{s}}_{\varepsilon}, \tau^{\mathrm{e}}_{\varepsilon}]\}$$

$$\sum_{l\in\mathbf{L}:\, i(l)=n} P'^{\mathrm{f}}_{\varepsilon,l,t} - \sum_{l\in\mathbf{L}:\, j(l)=n} P'^{\mathrm{f}}_{\varepsilon,l,t} = \sum_{h\in\mathbf{N}^{\mathrm{hrs}}:\, h=n} P'^{\mathrm{hrs}}_{\varepsilon,h,t} + \sum_{g\in\mathbf{N}^{\mathrm{gt}}:\, g=n} P'^{\iota}_{\varepsilon,g,t} + \sum_{h\in\mathbf{N}^{\mathrm{hrs}}:\, h=n} \sum_{m\in\mathbf{M}} P^{\mathrm{et}}_{\varepsilon,h,m,t} - P'^{\mathrm{D}}_{\varepsilon,i,t} - \sum_{e\in\mathbf{N}^{\mathrm{ec}}:\, e=n} P'^{\mathrm{ec}}_{\varepsilon,e,t} + P^{\mathrm{UD}}_{\varepsilon,i,t} \tag{14a}$$

$$\sum_{l\in\mathbf{L}:\, i(l)=n} Q'^{\mathrm{f}}_{\varepsilon,l,t} - \sum_{l\in\mathbf{L}:\, j(l)=n} Q'^{\mathrm{f}}_{\varepsilon,l,t} = \sum_{g\in\mathbf{N}^{gt}:\, g=n} Q'^{\iota}_{\varepsilon,g,t} - Q'^{\mathrm{D}}_{\varepsilon,i,t} + Q^{\mathrm{UD}}_{\varepsilon,i,t} \tag{14b}$$

$$V'_{\varepsilon,i(l),t} - V'_{\varepsilon,j(l),t} \geq 2(P'^{\mathrm{f}}_{\varepsilon,l,t} r_l + Q'^{\mathrm{f}}_{\varepsilon,l,t} x_l) - \mathcal{M} d^{\mathrm{L}}_{\varepsilon,l,t} \tag{14c}$$

$$V'_{\varepsilon,i(l),t} - V'_{\varepsilon,j(l),t} \leq 2(P'^{\mathrm{f}}_{\varepsilon,l,t} r_l + Q'^{\mathrm{f}}_{\varepsilon,l,t} x_l) + \mathcal{M} d^{\mathrm{L}}_{\varepsilon,l,t} \tag{14d}$$

$$(1 - d^{\mathrm{N}}_{\varepsilon,i,t}) P^{\mathrm{UD}}_{\varepsilon,i,t} = 0 \tag{14e}$$

The power generated by the on-site FC within the HRS during contingency operation scenarios is constrained by Equation (15a). The branch flow is subject to Equations (15b) and (15c), in which the term $(1 - d^{\mathrm{L}}_{\varepsilon,l,t})$ enforces the branch flow to be zero when the branch is offline.

$$\forall\{\varepsilon \in \Xi, h \in \mathbf{N}^{\mathrm{hrs}}, l \in \mathbf{L}, t \in \mathbf{T}^{\mathrm{c}}_{\varepsilon} : [\tau^{\mathrm{s}}_{\varepsilon}, \tau^{\mathrm{e}}_{\varepsilon}]\}$$

$$0 \leq P'^{\mathrm{hrs}}_{\varepsilon,h,t} = \eta^{\mathrm{fc}} \sigma^{\mathrm{fc}} g'^{\mathrm{hrs}}_{\varepsilon,h,t} \leq \mathrm{FC}^{\mathrm{U}}_{h} \tag{15a}$$

$$-\overline{P}^{\mathrm{f}}_{l}(1 - d^{\mathrm{L}}_{\varepsilon,l,t}) \leq P'^{\mathrm{f}}_{\varepsilon,l,t} \leq \overline{P}^{\mathrm{f}}_{l}(1 - d^{\mathrm{L}}_{\varepsilon,l,t}) \tag{15b}$$

$$-\overline{Q}^{\mathrm{f}}_{l}(1 - d^{\mathrm{L}}_{\varepsilon,l,t}) \leq Q'^{\mathrm{f}}_{\varepsilon,l,t} \leq \overline{Q}^{\mathrm{f}}_{l}(1 - d^{\mathrm{L}}_{\varepsilon,l,t}) \tag{15c}$$

Constraints (16a) and (16b) state that the operation status of the RCS ($d^{\mathrm{SU}}_{\varepsilon,l,t}$ or $d^{\mathrm{SD}}_{\varepsilon,l,t}$) depends on whether the RCS has been installed (s^{U}_{l} or s^{D}_{l}). Equations (16c) and (16d) enforce that an offline branch is isolated from the RCS side of the network ($d^{\mathrm{U}}_{\varepsilon,l,t}$ or $d^{\mathrm{D}}_{\varepsilon,l,t} = 0$) and the spread of the fault impacts is

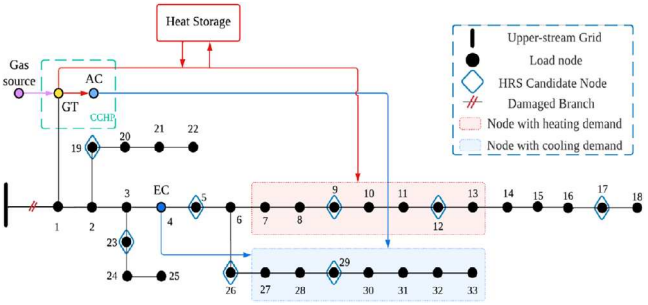

FIGURE 3 The basic setting of the proposed ISMS framework.

stopped if an RCS is installed (s^{U}_{l} or $s^{\mathrm{D}}_{l} = 1$) and is decided to open ($d^{\mathrm{SU}}_{\varepsilon,l,t}$ or $d^{\mathrm{SD}}_{\varepsilon,l,t} = 1$). Otherwise, if the RCS is closed ($d^{\mathrm{SU}}_{\varepsilon,l,t}$ or $d^{\mathrm{SD}}_{\varepsilon,l,t} = 0$), the feeder connected to node i is compromised as the fault's impact spreads ($d^{\mathrm{U}}_{\varepsilon,l,t}$ or $d^{\mathrm{D}}_{\varepsilon,l,t} = 1$). As defined in constraint (16e) for different contingency scenario ε, if branch l is damaged ($\varphi_{\varepsilon,l} = 1$) or either of the sending node $d^{\mathrm{N}}_{\varepsilon,i(l),t}$ or the receiving node $d^{\mathrm{N}}_{\varepsilon,j(l),t}$ of the branch is disabled ($d^{\mathrm{N}}_{\varepsilon,i(l),t} + d^{\mathrm{N}}_{\varepsilon,j(l),t} \geq 1$), the branch l is offline ($d^{\mathrm{L}}_{\varepsilon,l,t} = 1$). If either of the upstream or downstream sides of the branch connected to node i is disabled, the node is offline ($d^{\mathrm{N}}_{\varepsilon,n,t} = 1$), as enforced in Equation (16f).

$$\forall\{\varepsilon \in \Xi, n \in \mathbf{N}, l \in \mathbf{L}, t \in \mathbf{T}^{\mathrm{c}}_{\varepsilon} : [\tau^{s}_{\varepsilon}, \tau^{e}_{\varepsilon}]\}$$

$$d^{\mathrm{SU}}_{\varepsilon,l,t} \leq s^{\mathrm{U}}_{l} \tag{16a}$$

$$d^{\mathrm{SD}}_{\varepsilon,l,t} \leq s^{\mathrm{D}}_{l} \tag{16b}$$

$$d^{\mathrm{U}}_{\varepsilon,l,t} = (1 - d^{\mathrm{SU}}_{\varepsilon,l,t}) d^{\mathrm{L}}_{\varepsilon,l,t} \tag{16c}$$

$$d^{\mathrm{D}}_{\varepsilon,l,t} = (1 - d^{\mathrm{SD}}_{\varepsilon,l,t}) d^{\mathrm{L}}_{\varepsilon,l,t} \tag{16d}$$

$$d^{\mathrm{L}}_{\varepsilon,l,t} = \min\left((\varphi_{\varepsilon,l} + d^{\mathrm{N}}_{\varepsilon,i(l),t} + d^{\mathrm{N}}_{\varepsilon,j(l),t}), 1\right) \tag{16e}$$

$$d^{\mathrm{N}}_{\varepsilon,n,t} = \min\left(\left(\sum_{l\in\mathbf{L}:\, j(l)=n} d^{\mathrm{U}}_{\varepsilon,l,t} + \sum_{l\in\mathbf{L}:\, j(l)=n} d^{\mathrm{D}}_{\varepsilon,l,t}\right), 1\right) \tag{16f}$$

3 | NUMERICAL RESULTS

The performance of the proposed planning model for the hydrogen-based integrated seaport multi-energy system (ISMS) is tested on the IEEE 33-bus PDN as shown in Figure 3, with a single-line configuration and data available in [42]. There exist eight HRS candidate nodes across the system all containing V2G interfaces, one node installed with EC equipment, and one CCHP system, on which the suggested resilience-enhancing framework for the seaport multi-energy system is evaluated. The tests are conducted on a PC with an Intel Xeon E5-2620 v2 CPU and 16 GB RAM. The optimization problems are formulated with AMPL and solved with the state-of-the-art optimization solver Gurobi 9.0.2.

TABLE 2 Operation parameters of the studied seaport system.

System	Symbol	Value	Symbol	Value
CCHP	$\overline{G}$	500 m^3	C	13.067 kWh/m^3
	$\beta^{gt,e}/\beta^{gt,h}$	0.35/0.5	$\overline{P}^{ec}$	1800 kW
	β^{ac}/β^{ec}	0.6/0.8	δ^t	0.8
	$\overline{P}^t/\overline{H}^t/\overline{C}^t$	1660/3266/3000 kW	γ	0.001
	$S^{hs,ini}/\underline{S}^{hs}/\overline{S}^{hs}$	4500/3000/15,000 kWh	$\eta^{hs,c}/\eta^{hs,d}$	0.95
PDN	$\overline{P}^{v2g}$	4000 kW	δ^{sub}	0.8
	$\overline{P}^{sub}$	10,000 kW	λ^{UD}	10,000 \$/kW
HRS	λ^h/λ^{ph}	5.724/2.7 \$/kg	$\underline{P}^{p2h}/\overline{P}^{p2h}$	0/2000 kW
	$\underline{FC}/\overline{FC}$	0/2000 kW	$\varkappa_t^{p2h}/\varkappa_t^{ht}/\varkappa_t^{fc}$	6/28/20 \$/kW/year
	$\underline{SH}/\overline{SH}$	0/300 kg	σ^{p2h}	0.0287 kg/kW
	η^{fc}/η^{p2h}	0.5/0.79	σ^{fc}	23.8 kW/kg
	$\underline{PH}/\overline{PH}$	0/360 kg/d	$\vartheta^{p2h}/\vartheta^{ht}/\vartheta^{fc}$	35.1/52.5/120.7 \$/kW/year
	$\underline{g}_i^{hrs}$	1.5t/d (N5,9,12,17,19); 2t/d (N23,26,29)	ϑ^{hrs}	204,557.9 \$/year
RES	X_k^{res}	36 PV; 8 WT	$\varkappa_{k,t}^{res}$	0 \$/kW/year
	ϑ_k^{res}	PV=146.7 \$/kW/year; WT=210.3 \$/kW/year	$\overline{P}_k^{res}$	PV=300 kW; WT=500 kW
FCET	η^{et}	0.95	σ^{et}	15.7 kW/kg
	$\underline{E}/\overline{E}$	0/70 kg	$\varkappa_{m,t}^{et}$	900 \$/year
	TH_m	3.15 kg/h	$\overline{P}_m^{et}$	600 kW
	ϑ^{et}	12,6662 \$		
RCS	ϑ^{sw}	5000 \$		

While the proposed model is generic enough to accommodate any planning horizon, the planning horizon is here set to be 365 days. Four typical operational scenarios are defined to represent the daily operations in different seasons with different power, heating, and cooling demands. These scenarios correspond to a 24-h operation period specifically in January, April, July, and October, respectively, with equally likely probability. The power, heating, and cooling load profile is generated in the EnergyPlus software environment [43]. We generated 1000 different damage scenarios of up to $N-6$ contingencies in the PDN for contingency operations, where the scenarios are randomly selected using Monte Carlo simulations. The occurrence of each contingency scenario is assumed to be equally likely. Each damage scenario is randomly assigned with a contingency duration between the range of 2–10 h. To test the efficacy of the self-sustainability of the studied seaport system, it is assumed by default that no power flows from the upstream grid to the seaport PDN during contingency scenarios, and the damaged branches cannot be repaired during the contingency. The operation parameters for PDN, HRS, RES, RCS, FCET, and CCHP are listed in Table 2. The electricity and natural gas prices for the four different operation scenarios are shown in Figures 4 and 5, respectively [44]. Furthermore, the hourly heating and cooling demand under different scenarios are shown in Figure 6, while the 24-h available per-unit generation capacity factor of PV and

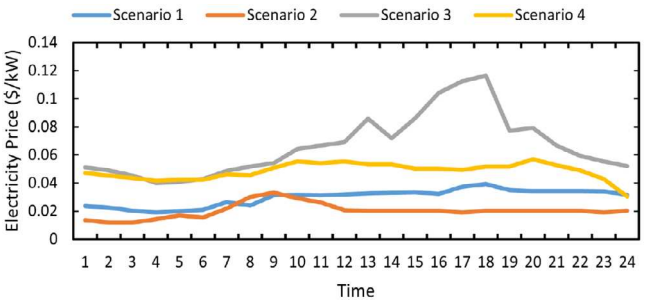

FIGURE 4 Hourly electricity prices in the four studied operation scenarios.

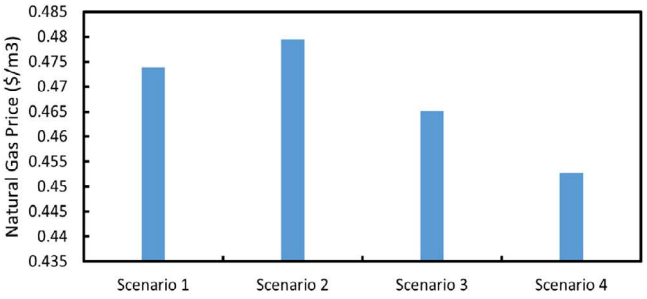

FIGURE 5 Natural gas prices in the four studied operation scenarios.

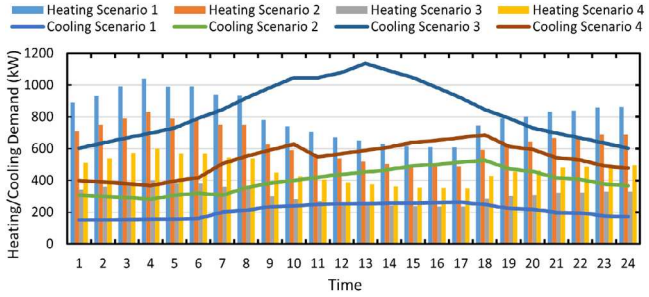

FIGURE 6 Hourly heating and cooling demand under different scenarios.

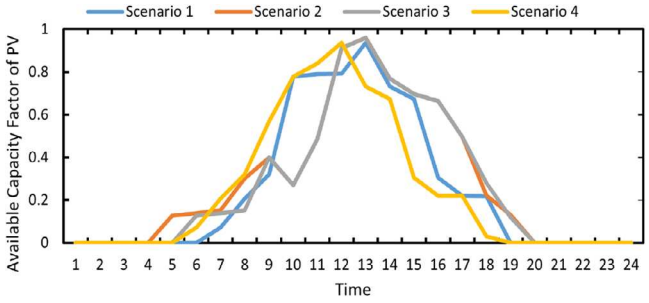

FIGURE 7 24-h available generation capacity factor of PV under different operation scenarios.

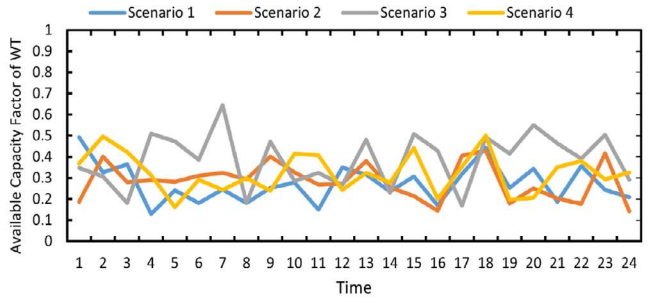

FIGURE 8 24-h available generation capacity factor of WT under different operation scenarios.

WT is presented in Figures 7 and 8. Note that, the PV data is simulated following the normal distribution, and WT data is simulated following the Weibull distribution [45, 46].

The performance of the proposed model is numerically verified through the following test cases:

- **Test Case 1**: Without additional assistance from FCETs ($\overline{N}^{et} = 0$) and no RCSs to be installed ($\overline{N}^{rcs} = 0$), relying only on HRSs' hydrogen production and distribution ($\overline{N}^{hrs} = 4$), and CCHP energy dispatch.
- **Test Case 2**: Without additional assistance from FCETs ($\overline{N}^{et} = 0$), relying solely on the HRSs' hydrogen production and distribution ($\overline{N}^{hrs} = 4$), RCSs operation ($\overline{N}^{rcs} = 20$), and CCHP energy dispatch.
- **Test Case 3**: With the coordination of HRSs' hydrogen production and distribution ($\overline{N}^{hrs} = 4$), RCSs operation ($\overline{N}^{rcs} = 20$), CCHP energy dispatch, and FCETs routing and power generation ($\overline{N}^{et} = 12$).

3.1 | Test case 1

The seaport PDN solely relies on pre-allocated HRSs and CCHP in the absence of FCET. The planning decision for HRSs, including P2H/RES/HT/FC within each HRS, is illustrated in Figure 9. Moreover, without RCS, the seaport grid lacks the ability to reconfigure and isolate the fault, rendering downstream nodes unable to receive power. In test case 1, the run time for the model is 2632 s, the capital investment cost amounts to $4,019,720, the annualized normal operation cost (operation/maintenance cost - sold hydrogen revenue) is found $4,100,260, and the annualized unserved demand cost is observed $78,771,300. The average total unserved power under 1000 contingency scenarios is 40.825% of the total power demand. Worth mentioning that, it occurred several times that only N2 is energized during the 6-order contingency scenarios in the network, and the rest of the nodes remain unserved. Due to the absence of RCSs in the system, the nodes and branches that are located downstream of the faulted line are impacted, leading to an overall increase in the extent of damage consequences. It is evident that even with CCHP and multiple HRSs in place, the seaport PDN is unable to achieve sufficient resilience in the event of severe damage to the network branches. The average unmet demand for heating and cooling stands at 6.182% and 19.69%, respectively. The installation of HS provides a backup heating energy source to be utilized in the case of contingency operations and explains why the heating demand is much lower than the unserved cooling demand. A large amount of unmet cooling demand is due to the inability to energize the node equipped with EC equipment under some contingency scenarios.

3.2 | Test case 2

In the absence of FCETs, the optimal planning decision for HRSs and RCSs is illustrated in Figure 10. The run time for test case 2 is 9702 s, which is much longer than that in test case 1 due to the large number of binary variables that are incorporated for switch control. The capital investment cost amounts to $4,531,320, and the annualized normal operation cost is $4,034,330. The total unserved demand penalty cost is $21,275,400, where the average overall unserved power compared to the total power demand under 1000 contingency scenarios is observed at 9.86%, with a penalty cost of $18,336,000. The average unmet demand for heating and cooling stands at 6.182% and 6.44%, respectively. Compared to test case 1, the unserved load was reduced significantly with the RCSs operation. Moreover, the decision to install RCSs is based on protecting branches with a high probability of failure. RCSs can isolate the faulted branches meanwhile allowing HRSs and CCHP to supply demand. Due to the limited number of HRSs

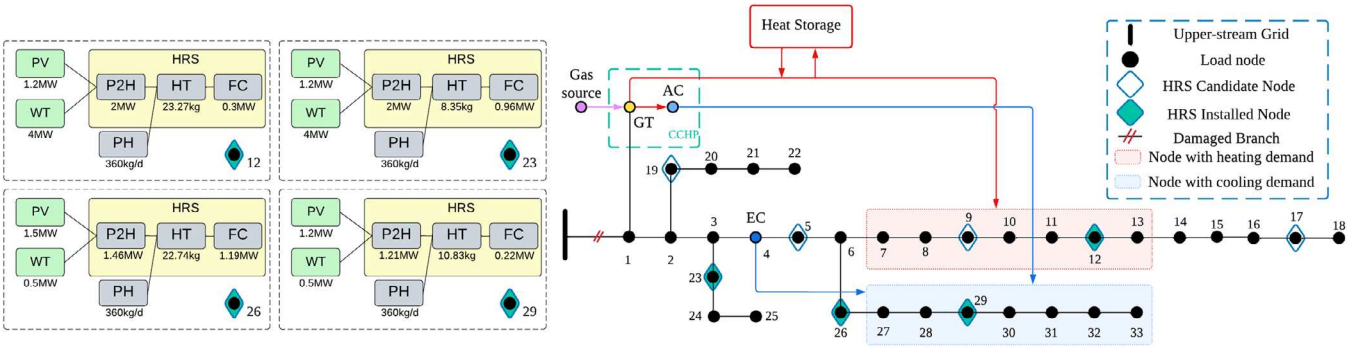

FIGURE 9 HRS planning decisions in test case 1.

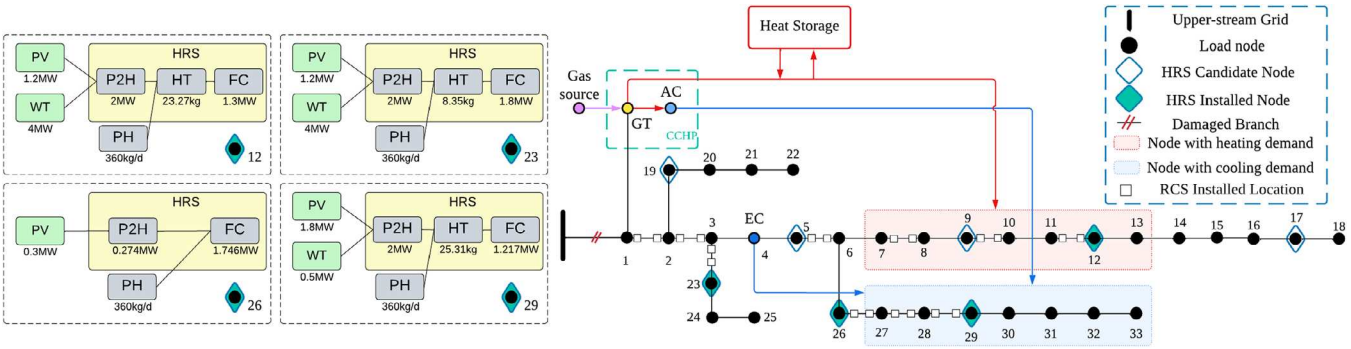

FIGURE 10 HRS and RCS planning decisions in test case 2.

that can be installed and the impact of damaged branches, certain nodes, namely N14, N19, and N20 under the contingency scenario with branches N4–N5, N13–N14, N2–N19, N6–N26 faulted, are left unserved. A notable finding is that even though branches N2–N19 and N13–N14 are more likely prone to failures when compared with other branches, no RCS has been installed on them. The rationale behind this is that there are no downstream source nodes for these branches, rendering it less worthwhile to isolate the faulted lines in the event that the nodes cannot be energized under any circumstance.

3.3 | Test case 3

Test case 3 considers the integration of FCETs, HRSs, and RCSs to enhance the resilience of the seaport PDN under contingency scenarios. Figure 11 illustrates the optimal planning decision of HRS and RCS with FCETs involved. The maximum number of FCETs that can be purchased is $\overline{N}^{ef} = 12$, all of which are invested in test case 3. The total capital investment cost for this configuration amounts to \$4,339,270, which is slightly less than that in test case 2. The installation capacity of the on-site FCs inside HRSs decreased due to the additional deployment of FCETs. The annualized normal operation cost is also reduced to \$4,067,010, which is more favourable compared to test case 2.

The numerical results demonstrate that the coordinated planning of HRSs, RCSs, CCHP, and FCETs in Test Case 3 significantly improves the system resilience. Specifically, the average overall unserved power in all contingency scenarios was reduced to 1.71%, with a penalty cost of \$3,035,200. The average unserved heating and cooling demands were also reduced to 2.66% and 1.37%, respectively. This represents a significant improvement compared to test cases 1 and 2, where the unserved demand was found much higher. All the highly-vulnerable branches are being protected by the RCSs as depicted in Figure 11, which allows the HRS candidate nodes that contain V2G interface to be unaffected by the fault occurrence and FCETs to remain capable of picking up the unserved loads within the isolated area. With the assumption that a limited number of HRSs, RCSs, and FCETs can be deployed in test case 3, a small load shedding is inevitable. The cost of unserved demand (per kW) was estimated to be \$10,000, which means that the seaport system only had on average approximately 303.52 kW demand unserved. This is a relatively small amount compared to the demand under normal operating conditions, indicating that the system resilience was greatly enhanced by the coordinated planning and operation of HRSs, RCSs, CCHP, and FCETs. Overall, the numerical results suggest that the integration of FCETs into the seaport PDN can significantly improve the system resilience and reduce the penalty cost of unserved demand.

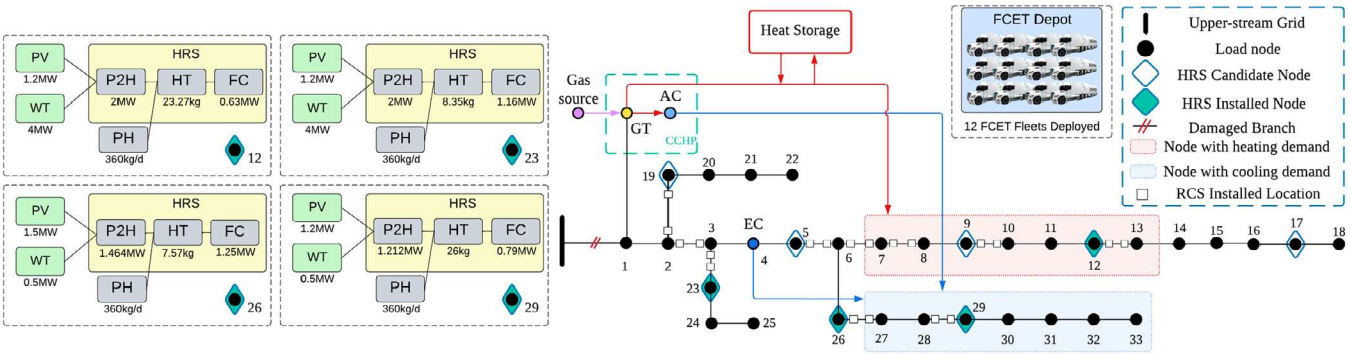

FIGURE 11 HRS, RCS, and FCET planning decision in test case 3.

4 | CONCLUSION

The integration of renewable energy sources, mobile, and stationary energy storage systems, and advanced switch control strategies has the potential to significantly enhance the resilience of seaport PDNs. By optimizing the deployment and scheduling of these resources, a reliable and affordable energy supply in both normal and emergency operating conditions could be ensured, while minimizing the impact incurred by catastrophic events. The presented case studies illustrated the efficacy of the proposed planning approach in a seaport multi-energy system, whereby integrating CCHP, HRSs, zero-emission FCETs, and RCSs along with renewable hydrogen generation and storage reduces the unserved power demand from 40.825% in test case 1 (relying solely on HRSs and CCHP) to 1.71% in test case 3 (coordinated operation of HRSs, RCSs, CCHP, and FCETs), while decreasing the unmet heating and cooling demand from 6.182% and 19.69% in test case 1 to 2.66% and 1.37% in test case 3. The proposed scenario-based optimization model enables the identification of an optimal mix of energy resources and contingency plans while taking into account various types of damage scenarios and cost considerations, offering a robust and sustainable solution for seaport development. Overall, the numerical results suggested that investing in resilience and low-carbon energy infrastructure can not only mitigate the risks of power outages but also generate economic benefits and environmental co-benefits for the seaport owners.

NOMENCLATURE

A. Abbreviation

PDN	Power distribution network
IPGS	Integrated power-gas system
DER	Distributed energy resource
EC	Electric chiller
GT	Gas turbine
HRS	Hydrogen refueling station
V2G	Vehicle to grid
FC	Fuel cell
FCET	Fuel cell electric truck
HT	Hydrogen tank
PH	Purified hydrogen
PV	Photovoltaic arrays
WT	Wind turbine
SOC	State of charge
HS	Heat storage
AC	Absorption chiller
CHP	Combined heat and power
CCHP	Combined cooling, heating, and power
RCS	Remote control switch

B. Sets and indices

$\mathbf{N}/i$	Set/index of nodes in the PDN
$\mathbf{N}^{ec}/\mathbf{N}^{hrs}/i$	Subset/index of EC/HRSs in the system
$\mathbf{N}^{sub}/\mathbf{N}^{gt}/i$	Subset/index of substation/CCHP in the system
$\mathbf{L}/l$	Set/index of branches in the PDN
$\mathbf{K}/k$	Set/index of candidate renewable energy components
$\mathbf{M}/m$	Set/index of FCETs
$\mathbf{\Gamma}/o$	Set/index on the segments of PDN separated into o regions
$\mathbf{\Omega}/w$	Set/index of normal operation scenarios
$\mathbf{\Xi}/\varepsilon$	Set/index of contingency scenarios
$\mathbf{T}^{n}/t$	Set/index of normal operation time slots
$\mathbf{T}^{c}_{\varepsilon}/t \in \{\tau^{s}_{\varepsilon}, \tau^{e}_{\varepsilon}\}$	Set/index of restoration time slots following a contingency occurrence

C. Variables

$G^{U}_{i}/SH^{U}_{i}/FC^{U}_{i}$	Installed capacity of P2H facility/HT /FC at HRS candidate node i
$x^{res}_{k,i}$	Integer variable indicating the installed number of RES units of type k at HRS candidate node i
$P^{p2h}_{w,i,t}/P'^{p2h}_{\varepsilon,i,t}$	Power input of P2H system in node i at time t under normal/contingency operation scenarios

$HF_{w,i,t}/HF'_{\varepsilon,i,t}$ Hydrogen outflow of HRS in node i at time t under normal/contingency operation scenarios

$P^{res}_{w,k,i,t}/P'^{res}_{\varepsilon,k,i,t}$ Power output of RES type k in node i at time t under normal/contingency operation scenarios

$g^{ph}_{w,i,t}/g'^{ph}_{\varepsilon,i,t}$ Purchased purified hydrogen in node i at time t under normal/contingency operation scenarios

$g^{sh}_{w,i,t}$ Sold hydrogen in node i at time t under normal operation scenario w

$\rho_{w,i,t}$ Hydrogen demand percentage ratio allocated to node i at time t under normal operation scenario w

$SH_{w,i,t}/SH'_{\varepsilon,i,t}$ Storage level of HTs in node i at time t under normal/contingency operation scenarios

$E_{\varepsilon,m,t}$ The hydrogen storage level of FCET m at time t under contingency scenario ε

$G_{w,t}/G'_{\varepsilon,t}$ Rate of natural gas consumption of GT at time t under normal/contingency operation scenarios

$g^{hrs}_{w,i,t}/g'^{hrs}_{\varepsilon,i,t}$ Released hydrogen masses from HRS i at time t under normal/contingency operation scenarios

$V_{w,i,t}/V'_{\varepsilon,i,t}$ Squared voltage level of node i at time t under normal/contingency operation scenarios

$P^{f}_{w,l,t}/Q^{f}_{w,l,t}$ Active/reactive power flow on branch l at time t under normal operation scenario w

$P'^{f}_{\varepsilon,l,t}/Q'^{f}_{\varepsilon,l,t}$ Active/reactive power flow on branch l at time t under contingency scenario ε

$P^{sub}_{w,i,t}/Q^{sub}_{w,i,t}$ Active/reactive power output from the upstream grid to node i at time t under normal operation scenario w

$P^{hrs}_{w,i,t}/P'^{hrs}_{\varepsilon,i,t}$ Active power output of HRS i at time t under normal/contingency operation scenarios

$P^{et}_{\varepsilon,i,m,t}$ Active power output of FCET m to node i at time t under contingency scenario ε

$g^{et}_{\varepsilon,i,m,t}$ Released hydrogen masses from FCET m to node i at time t under contingency scenario ε

$P^{ec}_{w,i,t}/P'^{ec}_{\varepsilon,i,t}$ Active power consumption of EC in node i at time t under normal /contingency operation scenarios

$P^{\iota}_{w,i,t}/Q^{\iota}_{w,i,t}$ Active/Reactive power output of the CCHP system in node i at time t under normal operation scenario w

$P'^{\iota}_{\varepsilon,i,t}/Q'^{\iota}_{\varepsilon,i,t}$ Active/Reactive power output of the CCHP system in node i at time t under contingency scenario ε

$H^{\iota}_{w,t}/H'^{\iota}_{\varepsilon,t}$ Heating output of the CCHP system at time t under normal/contingency operation scenarios

$C^{\iota}_{w,t}/C'^{\iota}_{\varepsilon,t}$ Cooling output of the CCHP system at time t under normal/contingency operation scenarios

$S^{hs}_{w,t}/S'^{hs}_{\varepsilon,t}$ SOC of the HS at time t under normal/contingency operation scenarios

$H^{hs,c}_{w,t}/H^{hs,d}_{w,t}$ Amount of heating energy charged /discharged by the HS at time t under normal operation scenario w

$H'^{hs,c}_{\varepsilon,t}/H'^{hs,d}_{\varepsilon,t}$ Amount of heating energy charged /discharged by the HS at time t under contingency scenario ε

$\alpha_{w,t}/\alpha'_{\varepsilon,t}$ The proportion of the heat energy produced by GT being used for CCHP heating output at time t under normal/contingency operation scenarios

$P^{UD}_{\varepsilon,i,t}/Q^{UD}_{\varepsilon,i,t}$ Unserved active/reactive power demand on node i at time t under contingency scenario ε

$H^{UD}_{\varepsilon,t}/C^{UD}_{\varepsilon,t}$ Unserved heating/cooling demand at time t under contingency scenario ε

z_i Binary variable, 1 if HRS is established on a candidate node i, 0 otherwise

y_m Binary variable, 1 if FCET m is purchased, 0 otherwise

$x^{et,s}_{\varepsilon,i,m,t}/x^{et,a}_{\varepsilon,i,m,t}$ Binary variable, 1 if FCET m stays /arrives at node i at time t under contingency scenario ε, 0 otherwise

$x^{et,g}_{\varepsilon,i,m}$ Binary variable, 1 if FCET m decides to go to node i under contingency scenario ε, 0 otherwise

$x^{et,o}_{\varepsilon,i,m,t}$ Binary variable, 1 if FCET m is on the way to node i at time t under contingency scenario ε, 0 otherwise

$\mu^{hs,c}_{w,t}/\mu^{hs,d}_{w,t}$ Binary variable, 1 if HS is charging/discharging at time t under normal operation scenario w, 0 otherwise

$\mu'^{hs,c}_{\varepsilon,t}/\mu'^{hs,d}_{\varepsilon,t}$ Binary variable, 1 if HS is charging /discharging at time t under contingency scenario ε, 0 otherwise

s^{U}_{l}/s^{D}_{l} Binary variable, 1 if RCS is installed at the upstream/downstream of branch l, 0 otherwise

$d^{L}_{\varepsilon,l,t}/d^{N}_{\varepsilon,i,t}$ Binary variable, 1 if branch(l)/node(i) is disabled at time t under contingency scenario ε, 0 otherwise

$d^{U}_{\varepsilon,l,t}/d^{D}_{\varepsilon,l,t}$ Binary variable, 1 if the upstream /downstream of branch l is compromised at time t under contingency scenario ε, 0 otherwise

$d^{SU}_{\varepsilon,l,t}/d^{SD}_{\varepsilon,l,t}$ Binary variable, 1 if the RCS at the upstream /downstream of branch l at time t is opened under contingency scenario ε, 0 otherwise

D. Parameters

$\lambda^{gas}_{w}/\lambda^{grid}_{w,t}$ Retail natural gas/electricity price at time t under normal operation scenario w

λ^{h}/λ^{ph} Retail price for HRSs sold hydrogen /purchased purified by-product hydrogen

λ^{UD} Unserved demand penalty cost

$\overline{N}^{hrs}/\overline{N}^{rcs}/\overline{N}^{et}$ Maximum number of HRS/RCS/FCET that can be deployed

$\beta^{gt,e}/\beta^{gt,h}$ Power/heating generation efficiency of GT
β^{ac}/β^{ec} Cooling generation efficiency of AC/EC
$\mathcal{C}$ Calorific value of natural gas
γ Self-release heat loss of HS
$H^{D}_{w,t}/C^{D}_{w,t}$ Total heating/cooling demand of the system at time t under normal operation scenario w
$H'^{D}_{\varepsilon,t}/C'^{D}_{\varepsilon,t}$ Total heating/cooling demand of the system at time t under contingency scenario ε
$\overline{G}$ Maximum volume of natural gas purchased per hour
$\overline{P}^{t}/\overline{H}^{t}/\overline{C}^{t}$ Maximum power/heating/cooling output of the CCHP system
$\overline{P}^{sub}$ Maximum power output from the upstream grid
$\overline{P}^{ec}$ Maximum power consumption of EC
$S^{hs,ini}/\underline{S}^{hs}/\overline{S}^{hs}$ Initial/minimum/maximum HS capacity
$\eta^{hs,c}/\eta^{hs,d}$ HS charging/discharging efficiency
$\underline{P}^{p2h}/\overline{P}^{p2h}$ Minimum/maximum output power capacity of the P2H facility
$\underline{SH}/\overline{SH}$ Minimum/maximum storage capacity of the HT
X^{res}_{k} Maximum number of RES units of type k that can be installed in HRS
η^{fc}/η^{et} Power generation efficiency of the on-site FC/FCET's on-board FC
σ^{fc}/σ^{et} Energy conversion rate of the on-site FC/FCET's on-board FC
η^{p2h}/σ^{p2h} Production efficiency/Conversion factor of the P2H system
$\psi^{res}_{w,k,t}/\psi'^{res}_{\varepsilon,k,t}$ Available capacity factor of RES type k at time t under normal/contingency operation scenarios
$\overline{g}^{hrs}_{i}$ Maximum daily hydrogen output of HRS at node i
$\overline{P}^{res}_{k}$ Unit power capacity of RES type k
$\overline{PH}$ Maximum capacity of available PH that can be purchased per day
$g^{D}_{w,o,t}$ Hydrogen refueling demands of sub-region o at time t under normal operation scenario w
$\overline{N}^{park}_{i}$ Maximum number of FCETs that can be parked at node i
$\underline{E}/\overline{E}$ Minimum/maximum storage capacity of on-board HT of FCET
TH_{m} Travel hydrogen energy consumption of FCET m
$\underline{FC}/\overline{FC}$ Minimum/maximum generation capacity of the on-site FC
r_{l}/x_{l} Resistance/reactance of branch l
$\overline{P}^{f}_{l}/\overline{Q}^{f}_{l}$ Maximum active/reactive power flow capacity of branch l
$P^{D}_{w,i,t}/Q^{D}_{w,i,t}$ Active/reactive power demand of node i at time t under normal operation scenario w
$P'^{D}_{\varepsilon,i,t}/Q'^{D}_{\varepsilon,i,t}$ Active/reactive power demand of node i at time t in contingency scenario ε
$\overline{P}^{v2g}$ Maximum power charging rate of V2G
δ^{t}/δ^{sub} Power factor of the CCHP/upstream grid power output
$TR_{i,m}$ Travel time of FCET to node i
$\overline{P}^{et}_{m}$ Maximum power output of FCET m
$\varkappa^{et}_{m,t}/\varkappa^{ht}_{t}/\varkappa^{fc}_{t}$ Fixed operation and maintenance cost of FCET fleet/HT/FC facility
$\varkappa^{p2h}_{t}/\varkappa^{res}_{k,t}$ Fixed operation and maintenance cost of unit capacity P2H/RES facility
$\vartheta^{p2h}/\vartheta^{ht}/\vartheta^{fc}$ Annualized investment cost of the unit capacity P2H facility/HT/FC
$\vartheta^{hrs}/\vartheta^{res}_{k}$ Capital investment cost of HRS/RES
$\vartheta^{sw}/\vartheta^{et}$ Capital investment cost of RCS/FCET
ϱ Number of days in the planning horizon
$\Theta_{\varepsilon,t}$ Indicator of the current time step within the entire contingency hours
$\varphi_{\varepsilon,l}$ Binary indicator, 1 if branch l is damaged, 0 otherwise
$\mathcal{P}^{n}/\mathcal{P}^{c}$ Occurrence probability of normal/contingency scenario within one year
$\mathcal{P}_{w}/\mathcal{P}'_{\varepsilon}$ Occurrence probability of each normal/contingency operation scenario in a day

AUTHOR CONTRIBUTIONS

Chengzhi Xie: Conceptualization; formal analysis; investigation; methodology; software; validation; visualization; writing—original draft; writing—review and editing. **Payman Dehghanian (GE)**: Funding acquisition; project administration; resources; supervision; writing—review and editing. **Abouzar Estebsari**: Investigation; supervision; writing—review and editing.

CONFLICT OF INTEREST STATEMENT

The authors declare no conflicts of interest.

DATA AVAILABILITY STATEMENT

The data that support the findings of this study are available from the corresponding author upon reasonable request.

ORCID

Chengzhi Xie https://orcid.org/0000-0002-2686-5980
Payman Dehghanian https://orcid.org/0000-0003-2237-4284

REFERENCES

1. Bakar, N.N.A., Guerrero, J.M., Vasquez, J.C., Bazmohammadi, N., Yu, Y., Abusorrah, A., Al-Turki, Y.A.: A review of the conceptualization and operational management of seaport microgrids on the shore and seaside. Energies 14(23), 7941 (2021)
2. Fang, S., Wang, Y., Gou, B., Xu, Y.: Toward future green maritime transportation: an overview of seaport microgrids and all-electric ships. IEEE Trans. Veh. Technol. 69(1), 207–219 (2020)
3. Fang, S., Wang, H.: Optimization-based energy management for multi-energy maritime grids. Springer Nature, Cham (2021)

4. Sadiq, M., Ali, S.W., Terriche, Y., Mutarraf, M.U., Hassan, M.A., Hamid, K., Ali, Z., Sze, J.Y., Su, C.-L., Guerrero, J.M.: Future greener seaports: A review of new infrastructure, challenges, and energy efficiency measures. IEEE Access 9, 75568–75587 (2021)
5. Sherman, R.: Seaport governance in the united states and canada. American Association of Port Authorities, Alexandria, VA (2000)
6. Yao, S., Gu, W., Lu, S., Zhou, S., Wu, Z., Pan, G., He, D.: Dynamic optimal energy flow in the heat and electricity integrated energy system. IEEE Trans. Sustainable Energy 12(1), 179–190 (2021)
7. Li, Y., Wang, J., Han, Y., Zhao, Q.: Generalized modeling and coordinated management of energy hub incorporating wind power and demand response. In: 2019 Chinese Control And Decision Conference (CCDC), pp. 4214–4219. IEEE, Piscataway, NJ (2019)
8. Wang, X., Huang, W., Wei, W., Tai, N., Li, R., Huang, Y.: Day-ahead optimal economic dispatching of integrated port energy systems considering hydrogen. IEEE Trans. Ind. Appl. 58(2), 2619–2629 (2022)
9. Duan, Z., Yan, Y., Yan, X., Liao, Q., Zhang, W., Liang, Y., Xia, T.: An MILP method for design of distributed energy resource system considering stochastic energy supply and demand. Energies 11(1), 22 (2018)
10. Li, N., Zhao, X., Shi, X., Pei, Z., Mu, H., Taghizadeh-Hesary, F.: Integrated energy systems with CCHP and hydrogen supply: a new outlet for curtailed wind power. Appl. Energy 303, 117619 (2021)
11. Pu, Y., Chen, W., Zhang, R., Liu, H.: Optimal operation strategy of port integrated energy system considering demand response. In: 2020 IEEE 4th Conference on Energy Internet and Energy System Integration (EI2), pp. 518–523. IEEE, Piscataway, NJ (2020)
12. Sun, T., Lu, J., Li, Z., Lubkeman, D.L., Lu, N.: Modeling combined heat and power systems for microgrid applications. IEEE Trans. Smart Grid 9(5), 4172–4180 (2018)
13. Smith, T., Jalkanen, J., Anderson, B., Corbett, J., Faber, J., Hanayama, S., Pandey, A.: Third IMO Greenhouse Gas Study 2014, International Maritime Organization, London (2014)
14. Zandi, M., Payman, A., Martin, J.-P., Pierfederici, S., Davat, B., Meibody-Tabar, F.: Energy management of a fuel cell/supercapacitor/battery power source for electric vehicular applications. IEEE Trans. Veh. Technol. 60(2), 433–443 (2011)
15. Hu, X., Murgovski, N., Johannesson, L.M., Egardt, B.: Optimal dimensioning and power management of a fuel cell/battery hybrid bus via convex programming. IEEE/ASME Trans. Mechatron. 20(1), 457–468 (2015)
16. Shao, Z., Cao, X., Zhai, Q., Guan, X.: Risk-constrained planning of rural-area hydrogen-based microgrid considering multiscale and multi-energy storage systems. Appl. Energy 334, 120682 (2023)
17. Cao, X., Sun, X., Xu, Z., Zeng, B., Guan, X.: Hydrogen-based networked microgrids planning through two-stage stochastic programming with mixed-integer conic recourse. IEEE Trans. Autom. Sci. Eng. 19(4), 3672–3685 (2022)
18. Jenn, A., Highleyman, J.: Distribution grid impacts of electric vehicles: a California case study. iScience 25(1), 103686 (2022)
19. Aljehane, N.O., Mansour, R.F.: Optimal allocation of renewable energy source and charging station for PHEVs. Sustainable Energy Technol. Assess. 49, 101669 (2022)
20. Wang, W., Liu, L., Liu, J., Chen, Z.: Energy management and optimization of vehicle-to-grid systems for wind power integration. CSEE J. Power Energy Syst. 7(1), 172–180 (2021)
21. Xu, Y., Liu, C.-C., Schneider, K.P., Ton, D.T.: Placement of remote-controlled switches to enhance distribution system restoration capability. IEEE Trans. Power Syst. 31(2), 1139–1150 (2016)
22. Hassanzadeh, E., Hajiabadi, M.E., Samadi, M., Lotfi, H.: Improving the resilience of the distribution system using the automation of network switches. J. Eng. 2023(2), e12238 (2023)
23. Taheri, B., Safdarian, A., Moeini-Aghtaie, M., Lehtonen, M.: Distribution system resilience enhancement via mobile emergency generators. IEEE Trans. Power Delivery 36(4), 2308–2319 (2021)
24. Li, Y., Zhang, H., Liang, X., Huang, B.: Event-triggered-based distributed cooperative energy management for multienergy systems. IEEE Trans. Ind. Inf. 15(4), 2008–2022 (2019)
25. Song, T., Li, Y., X.-P.Zhang, Wu, C., Li, J., Guo, Y., Gu, H.: Integrated port energy system considering integrated demand response and energy interconnection. Int. J. Electr. Power Energy Syst. 117, 105654 (2020)
26. Li, G., Zhang, R., Jiang, T., Chen, H., Bai, L., Li, X.: Security-constrained bi-level economic dispatch model for integrated natural gas and electricity systems considering wind power and power-to-gas process. Appl. Energy 194, 696–704 (2017)
27. Khani, H., Farag, H.E.Z.: Optimal day-ahead scheduling of power-to-gas energy storage and gas load management in wholesale electricity and gas markets. IEEE Trans. Sustainable Energy 9(2), 940–951 (2017)
28. Bai, L., Li, F., Jiang, T., Jia, H.: Robust scheduling for wind integrated energy systems considering gas pipeline and power transmission N–1 contingencies. IEEE Trans. Power Syst. 32(2), 1582–1584 (2016)
29. Poudel, S., Dubey, A.: Critical load restoration using distributed energy resources for resilient power distribution system. IEEE Trans. Power Syst. 34(1), 52–63 (2019)
30. Ranjbar, H., Hosseini, S.H., Zareipour, H.: Resiliency-oriented planning of transmission systems and distributed energy resources. IEEE Trans. Power Syst. 36(5), 4114–4125 (2021)
31. Zhang, B., Dehghanian, P., Kezunovic, M.: Optimal allocation of pv generation and battery storage for enhanced resilience. IEEE Trans. Smart Grid 10(1), 535–545 (2019)
32. Arjomandi-Nezhad, A., Fotuhi-Firuzabad, M., Moeini-Aghtaie, M., Safdarian, A., Dehghanian, P., Wang, F.: Modeling and optimizing recovery strategies for power distribution system resilience. IEEE Syst. J. 15(4), 4725–4734 (2021)
33. Wu, X., Liu, J., Men, Y., Chen, B., Lu, X.: Optimal energy storage system and smart switch placement in dynamic microgrids with applications to marine energy integration. IEEE Trans. Sustainable Energy 14(2), 1205–1216 (2023)
34. Izadi, M., Safdarian, A.: A MIP model for risk constrained switch placement in distribution networks. IEEE Trans. Smart Grid 10(4), 4543–4553 (2019)
35. Anokhin, D., Dehghanian, P., Lejeune, M.A., Su, J.: Mobility-as-a-service for resilience delivery in power distribution systems. Prod. Oper. Manag. 30(8), 2492–2521 (2021)
36. Su, J., Anokhin, D., Dehghanian, P., Lejeune, M.A.: On the use of mobile power sources in distribution networks under endogenous uncertainty. IEEE Trans. Control Network Syst. 1–12 (2023). https://doi.org/10.1109/TCNS.2023.3256278
37. Li, Z., Tang, W., Lian, X., Chen, X., Zhang, W., Qian, T.: A resilience-oriented two-stage recovery method for power distribution system considering transportation network. Int. J. Electr. Power Energy Syst. 135, 107497 (2022)
38. Dong, Y., Zheng, W., Cao, X., Sun, X., He, Z.: Co-planning of hydrogen-based microgrids and fuel-cell bus operation centers under low-carbon and resilience considerations. Appl. Energy 336, 120849 (2023)
39. Saboori, H., Mehrjerdi, H., Jadid, S.: Mobile battery storage modeling and normal-emergency operation in coupled distribution-transportation networks. IEEE Trans. Sustainable Energy 13(4), 2226–2238 (2022)
40. Baran, M., Wu, F.: Network reconfiguration in distribution systems for loss reduction and load balancing. IEEE Trans. Power Delivery 4(2), 1401–1407 (1989)
41. Hijazi, H., Thiébaux, S.: Optimal distribution systems reconfiguration for radial and meshed grids. Int. J. Electr. Power Energy Syst. 72, 136–143 (2015)
42. Baran, M., Wu, F.: Network reconfiguration in distribution systems for loss reduction and load balancing. IEEE Trans. Power Delivery 4(2), 1401–1407 (1989)
43. The National Renewable Energy Laboratory (NREL): Energyplus. https://energyplus.net/ Accessed 16 Feb 2023
44. The National Grid USA Service Company.: Rate & pricing of electricity and natural gas. https://www.nationalgridus.com/Upstate-NY-Business/Rates/Supply-Costs. Accessed 9 Mar 2023

45. Dehghanian, P., Kezunovic, M.: Probabilistic decision making for the bulk power system optimal topology control. IEEE Trans. Smart Grid 7(4), 2071–2081 (2016)
46. Alhazmi, M., Dehghanian, P., Wang, S., Shinde, B.: Power grid optimal topology control considering correlations of system uncertainties. IEEE Trans. Ind. Appl. 55(6), 5594–5604 (2019)
47. McCormick, G.P.: Computability of global solutions to factorable nonconvex programs: Part I–Convex underestimating problems. Math. Program. 10(1), 147–175 (1976)
48. Gupte, A., Ahmed, S., Cheon, M.S., Dey, S.: Solving mixed integer bilinear problems using MILP formulations. SIAM J. Optim. 23(2), 721–744 (2013)
49. Dombrowski, J.: Global optimization - mccormick envelopes. https://arch.library.northwestern.edu/concern/generic_works/ft848q804?locale=en. Accessed 15 Mar 2023
50. Scott, J.K., Stuber, M.D., Barton, P.I.: Generalized mccormick relaxations. J. Global Optim. 51(4), 569–606 (2011)

How to cite this article: Xie, C., Dehghanian, P., Estebsari, A.: Fueling the seaport of the future: Investments in low-carbon energy technologies for operational resilience in seaport multi-energy systems. IET Gener. Transm. Distrib. 18, 248–265 (2024). https://doi.org/10.1049/gtd2.13058

APPENDIX A: LINEARIZATION OF THE NONLINEAR TERMS

The proposed model is nonconvex due to the nonlinear constraints (4b), (4c), (10b), (10c), (14e), (16c)–(16f). The nonlinear terms include the product of two binary variables, the product of a binary variable with a continuous variable, and the min() function.

To reformulate the min() function, let x and y be binary variables. Equation (A1a) can be equivalently expressed using Equations (A1b) and (A1c). If $y = 0$, then Equation (A1b) forces x to be 0. Similarly, if $y = 1$, then Equation (A1c) enforces x to be 1, satisfying the desired condition.

$$x = \min(y, 1) \tag{A1a}$$

$$x \leq y \tag{A1b}$$

$$(x - 1)y = 0 \tag{A1c}$$

However, the above reformulation results in the product of two binary variables (xy). The product of two binary variables can be linearized as Equations (A2b)–(A2d) by introducing a new auxiliary binary variable z.

$$z = xy \tag{A2a}$$

$$z \leq x \tag{A2b}$$

$$z \leq y \tag{A2c}$$

$$z \geq x + y - 1 \tag{A2d}$$

The McCormick envelopes [47, 48] offer a linearization technique to transform the product of a binary variable and a continuous variable into a linear form. It is important to note that in this particular case, both terms ($G_{w,t}$ and $\alpha_{w,t}$) are continuous variables, and the McCormick inequalities can only provide a linear relaxation. While McCormick relaxations offer quality approximations, they aren't always exact [49, 50]. Accordingly, our numerical analysis emphasizes instances where the results post-relaxation closely matched exact solutions with the optimality gap lower than 0.01%. By introducing the non-negative auxiliary variable ς_t, constraints (4b) and (4c) can be replaced by the following linear constraints (A3a)–(A3f).

$$\forall\{w \in \mathbf{\Omega}, t \in \mathbf{T}^{\mathrm{n}}\}$$

$$H_t^t = \varsigma_t \mathcal{C} \beta^{\mathrm{gt},b} \tag{A3a}$$

$$C_t^t = G_{w,t} \mathcal{C} \beta^{\mathrm{ac}} \beta^{\mathrm{gt,h}} - \varsigma_t \mathcal{C} \beta^{\mathrm{ac}} \beta^{\mathrm{gt,h}} \tag{A3b}$$

$$\varsigma_t \geq 0 \tag{A3c}$$

$$\varsigma_t \geq G_{w,t} + \overline{G} \alpha_{w,t} - \overline{G} \tag{A3d}$$

$$\varsigma_t \leq G_{w,t} \tag{A3e}$$

$$\varsigma_t \leq \overline{G} \alpha_{w,t} \tag{A3f}$$

By using the aforementioned linearization methods, all the nonlinear constraints can be reformulated into the linear form and can be solved directly by the Gurobi solver.